101p

N63 17222

Code-1

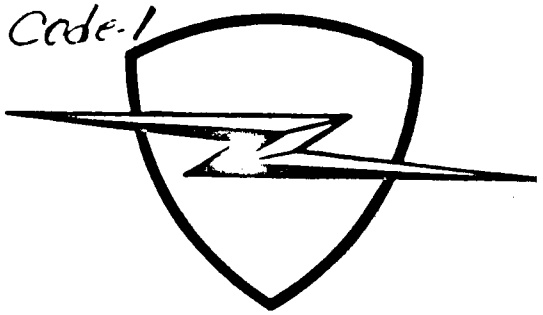

Report Number 1414

A Comparison of Thin Coatings of Phenolic Nylon and "THERMO-LAG" T-500 During Exposure to Low Convective Heat Fluxes of Long Duration

---

Prepared for

NATIONAL AERONAUTICS AND
SPACE ADMINISTRATION
Manned Spacecraft Center
Houston 1, Texas

OTS PRICE

XEROX $ [redacted]

MICROFILM $ [redacted]

ELECTRONICS AND AVIONICS DIVISION

EMERSON ELECTRIC
MANUFACTURING COMPANY
8100 Florissant Avenue
St. Louis 36, Missouri

Report Number 1414

A Comparison of Thin Coatings of Phenolic Nylon and "THERMO-LAG" T-500 During Exposure to Low Convective Heat Fluxes of Long Duration

Prepared for

NATIONAL AERONAUTICS AND SPACE ADMINISTRATION
Manned Spacecraft Center
Houston 1, Texas

21 November 1962

ELECTRONICS AND AVIONICS DIVISION

EMERSON ELECTRIC MANUFACTURING COMPANY
8100 Florissant Avenue
St. Louis 36, Missouri

This report is submitted to The National Aeronautics And Space Administration, Manned Spacecraft Center, Houston 1, Texas, by The Emerson Electric Manufacturing Company, St. Louis, Missouri in accordance with the requirements, terms, and conditions of Contract NAS 9-706, Control No. 3-420-202-998.

ABSTRACT 17222

The experimental determination of the relative effectiveness of two thermal barrier materials was undertaken to provide data leading to a minimum weight solution to the thermal protection problem presented by the afterbody areas of a manned superorbital re-entry vehicle. The materials investigated were "THERMO-LAG" T-500, produced by Emerson Electric, and a low-density nylon-reinforced phenolic ablating formulation. The materials were applied to test models on an equivalent weight basis, the ablative material weights ranging from 0.03 to 0.18 pound per square foot.

Tests were conducted in a Mach 3, 200-kw air-stabilized arc jet at two conditions simulating thermal environments to be encountered by the vehicle.

The test results showed "THERMO-LAG" T-500 to be the superior material for the application, both thermally and mechanically. "THERMO-LAG" maintained the temperature of the substrate steel at or below its sublimation temperature of 530°F., while under identical conditions, application weights, and exposure durations, the phenolic nylon coating permitted temperatures to approach 900°F. At a heat flux of 30 BTU/ft^2 sec and an enthalpy of 3500 BTU/lb, the "THERMO-LAG" maintained original model configuration and formed an essentially nonreceding debris matrix in the stagnation region. The phenolic nylon models, under identical conditions, were subject to major configuration change. Cracking and spalling of the phenolic nylon coating material was observed during certain of the tests.

TABLE OF CONTENTS

TABLE OF CONTENTS (CONT)

LIST OF ILLUSTRATIONS

LIST OF ILLUSTRATIONS (CONT)

LIST OF ILLUSTRATIONS (CONT)

OBJECTIVE

- The objective of the program conducted under Contract NAS 9-706 was to perform a series of tests, at heating conditions typical of the Apollo afterbody, by which to make a direct comparison between the performance of two thermal protection materials. The two materials to be tested were "THERMO-LAG" T-500 and a low-density ablator composed of 47.0 percent Zytel 103 nylon powder, 23.0 percent Bakelite BRP 5549 phenolic resin, 25.0 percent phenolic microballoons, and 5.0 percent eccospheres (silica balloons), SI grade.

INTRODUCTION

The establishment of the relative efficiency of ablative thermal barrier materials is requisite to the attainment of a minimum weight solution to a given thermal protection problem. This document reports such a comparison.

Two ablative thermal barrier materials of demonstrated superior performance were selected by NASA for testing. The purpose of the test program was to establish, by direct flight simulation comparison, the relative efficiency of these two materials as thermal protective systems during exposure to certain thermal conditions expected to be encountered by the afterbody of a typical low $\frac{W}{C_D A}$, low $\frac{L}{D}$, vehicle during shallow-angle entry to the earth's atmosphere.

SYMBOLS

D = Drag force (lb)
A = Area (ft^2)
B = Slope of dissociation curve with temperature (BTU/lb °R)
C_D = Coefficient of drag (dimensionless)
F = Configuration factor for radiant heat interchange (dimensionless)
H = Heat of combustion BTU/lb
H_{eff} = Effective heat of ablation (BTU/lb)
L = Lift force (lb)
Q = Heat of vaporization, fusion, or sublimation (BTU/lb)
R = Radius of curvature (ft)
O_2 = Mass fraction of oxygen present in boundary layer (dimensionless)
T = Temperature (°R)
W = Weight (lb)
c = Specific heat (BTU/lb °R)
h = Enthalpy (BTU/lb), or film coefficient of heat transfer (BTU/ft^2 °R sec)
k = Thermal conductivity (BTU ft/ft^2 °R sec)
m = Mass per unit area (lb/ft^2)
p = Pressure (Atmospheres)
q = Heat Flux (BTU/ft^2 sec)

$$q^{**} = \frac{\int_{t=0}^{t=t} q\,dt}{Wa/A}$$

Ablative efficiency, where q^{**}, at $t=t$, is plotted versus temperature, at $t=t$, for constant values of Wa/A. $t=0$ at start of test, and $t=t$ at time that temperature is plotted.

t = Time (sec)
x = Linear recession of model (ft)
α = Transpiration factor, fractional temperature rise of gases (dimensionless)
β = Fractional amount of dissociation on boundary layer (dimensionless)
Θ = Time in seconds for substrate to attain 99% of driving temperature (Appendix C)
ϵ = Emissivity (dimensionless)
σ = Stefan Boltzman constant (BTU/ft^2 hr $°F^4$)
$\xi = \frac{\rho_a - \rho_q}{\rho_a}$ Mass fraction of material gassified (dimensionless)
ρ = Density (lb/ft^3)

SUBSCRIPTS.

a = Ablative material
c = Cold Wall 5/8-inch diameter calorimeter
d = Driving Temperature, or debris material changing to gas at interface "m"
qd = Debris material transpiring into boundary layer
qv = Virgin material gases transpiring through debris layer

SUBSCRIPTS (Continued)

$_i$ = Initial conditions, or interface between debris and virgin material
$_m$ = Model
$_o$ = Nozzle static pressure at exit
$_{o'}$ = Stagnation pressure measured by pitot probe
$_r$ = Re-radiated from model
$_{rec}$ = Recovery temperature or conditions
$_s$ = Transient calorimeter sensor, or steel cylindrical heat sink
$_t$ = Total or stagnation conditions
$_v$ = Virgin material changing into gas or liquid at interface "i"
$_F$ = Heat of fusion
$_S$ = Heat of sublimation
$_V$ = Heat of vaporization

MATERIALS

The materials tested in accordance with the requirements of Contract NAS 9-706 were as follows:

1. "THERMO-LAG" T-500, a subliming, paint-like, moldable material designed for thermal protection and temperature control of hyperperformance vehicles. "THERMO-LAG" T-500 sublimes at a predesigned fixed temperature (530°F), thus limiting the temperature of any substrate material to a known and unchanging maximum. As the material sublimes, the products of decomposition of certain additives form a stable debris layer. This debris layer is capable of achieving a high surface temperature through which the sublimate gases transpire. The combination of latent heat of sublimation, thermal diffusivity, mass transfer, injection into the boundary layer of low molecular weight gases, further endothermic sublimate dissociation in the debris matrix, and reradiation from the high-temperature debris surface combine to form a highly efficient heat blocking mechanism. Since the temperature of sublimation is not a function of heat input, the "THERMO-LAG" materials perform a thermostatic temperature controlling function and are superior in this regard to other ablative heat-shielding processes in current use.
2. A low-density ablator formulated from 47.0 percent Zytel 103 nylon powder, 23.0 percent Bakelite BRP 5549 phenolic resin, 25.0 percent phenolic microballons, and 5.0 percent eccospheres (silica balloons), SI grade.

APPARATUS

PLASMA JET.

The test work reported herein was conducted in the Plasmadyne Corporation hyperthermal test system at Santa Ana, California. The system consists of a 200-kilowatt arc plasma generator, mixing chamber, aerodynamic nozzle, Mach 3 test section, and associated gas, vacuum, coolant, and electrical systems. Instrumentation is provided for accurate determination of the thermal environment in the test section. A detailed description of the hyperthermal test system appears in Appendix B.

TEST MODELS.

Figure 7 shows the details of test model construction and instrumentation. The models consisted of a 2-1/2-inch diameter cylinder with a hemispherical nose section. The over-all length of the cylindrical and hemispherical assembly was four inches. A sting mounting subassembly was bonded to the back of the model to provide a means of holding the model in the plasma stream. The cylindrical section was prepared by applying the ablative material to a steel sleeve ground to a thickness of 0.030 plus or minus 0.0005 inch. The phenolic nylon test material was machined to a hollow tube configuration, bonded to the steel sleeve, and machined to the desired external dimension. The "THERMO-LAG" material was applied by spraying to the steel sleeve, heat-cured, and then machined to the proper external dimension. (Two thermocouples 180 degrees apart were swaged to the steel sleeve one inch from the aft end of the sleeve.) Thermocouple junctions were positioned to record the temperature at the steel substrate. The hemispherical nose sections were provided with a thermocouple peened to a 5/16-inch diameter copper disc which was 0.030 inch thick. The copper disc and thermocouple junction were positioned 1.250 inches aft of the stagnation point.

A finished phenolic nylon test model is shown in Figure 8.

CALORIMETERS.

Two calorimeters were fabricated for the program (See Figure 9.) The body of Calorimeter Number 1 was made of copper for use under low heat flux conditions. Calorimeter Number 4 was constructed of graphite for use under high heat flux conditions. Graphite sensors equipped with thermocouples were press-fitted into cavities in the calorimeter body until only the thin lip around the outside heated surface of the calorimeter body was in contact with the sensor plug, thus minimizing two-dimensional heat conduction into the cool calorimeter body. The heat flux incident upon the surface of the sensor could be measured, therefore, by the rate of heat storage in the sensor. A schematic diagram of the calorimeter design is presented in Figure 7. Figure 7 also depicts the configuration of the calorimeter body cavities into which the sensors were introduced.

TEST PROCEDURE

All tests were conducted in the following sequence:

1. Photographs of the test models were taken.
2. Over-all model dimensions were recorded.
3. The model was installed in the hyperthermal test facility sting mounting.
4. The model was then aligned with the jet centerline.
5. The oscillograph internal timing mechanism was calibrated by a known duration square wave electrical current fed into an oscillograph galvanometer. The duration as indicated by the timing mechanism was recorded along with the known duration to provide scale factors for later use in data reduction. No discrepancies were noted during the program.
6. A precision potentiometer was used to check each thermocouple for discontinuity and to measure thermocouple lead resistance.
7. The model was lowered from the position shown in Figure 4 to a position out of line with the nozzle exit.
8. The test section was then evacuated to the desired pressure.
9. The arc was struck and stabilized at the desired power level.
10. Pressure was determined by means of a water-cooled pitot probe.
11. Heat transfer to a 5/8-inch water-cooled copper calorimeter was measured.
12. All tunnel operating parameters were then recorded. These included pressures; temperatures; flow rates of water, nitrogen, and oxygen; etc. Operating conditions were monitored throughout the test.
13. Cooling water flow to the sting mounting was initiated and the model pneumatically inserted into the plasma stream. At this time, a stopwatch, the recording oscillograph, and a color motion picture camera were started.
14. Measurements of model surface temperature in the stagnation point region were made with an optical pyrometer.
15. At the conclusion of the designed test period, the arc was extinguished. The test model was permitted to remain in position for a cooling period prior to removal from the test chamber.

Post-test examination of the models included:

1. Weighing the models.
2. Photographing the models.
3. Sectioning of the stagnation region of the models, and performing a microscopic inspection of the char in the stagnation region.
4. Measuring the debris layer thickness and recession of the virgin material.
5. Sectioning of the model in the test area over thermocouples 2 and 3 and microscopically examining the material to qualitatively determine its composition.

DATA REDUCTION

STAGNATION POINT.

HEAT FLUX.

Heat flux to the test model was determined by ratioing the calibrating flux (obtained before each run) to the 5/8-inch calorimeter. The following equation was used:

$$q_m = q_c \left(\frac{h_t - h_m}{h_t - h_c}\right)\sqrt{\frac{R_c}{R_m}}$$

DATA.

Recession rates of virgin material were considered to be linear with time. These recession rates were obtained by dividing the total recession by the duration of the test.

The heat of ablation, H_{eff}, was evaluated by:

a. Dividing the model hot wall convective heat flux by the mass ablation rate determined from the recession rate presented above.

$$H_{eff} = \frac{q_m}{(dx/dt)\rho}$$

b. Subtracting the reradiated heat flux from the hot-wall convective heat flux, and then dividing by the mass ablation rate.

$$H_{eff} = \frac{q_m - q_r}{(dx/dt)\rho}$$

Reradiated heat flux was determined by using the surface energy obtained by direct measurement.

SIDE WALLS.

HEAT FLUX.

Heat flux was evaluated by transient hot-wall calorimetry. Rate-of-heat transfer to the sensor face was determined accurately from the rate of heat transfer into it, and was monitored by a 28-gage chromel-alumel thermocouple within the sensor and recorded on an oscillograph. The slopes of these traces were evaluated at several temperatures throughout the test. The incident heat flux was evaluated from:

$$q_s = \frac{1}{A_s} W_s c_s \frac{dT_s}{dt}$$

DATA.

Data reduction for side walls of the models was accomplished by a q^{**} parameter. This parameter is a measure of the total heat-pulse-per-pound of material applied to the side walls.

$$q^{**} = \frac{(q)(t)}{W_s/A} (BTU/lb)$$

This parameter was plotted versus substrate temperature for each model. Since the weights per unit area of the coatings of the two materials were reasonably close for each pair of models tested, it was possible to compare, on single graphs, the relative protection offered by equal weights of each material for the several exposures to the plasma stream. These curves are presented in Figures 47 through 53. The criterion for assessing material thermal efficiency was minimum backside temperature rise for equal exposure to identical thermal environment.

THERMAL ENVIRONMENT AND TUNNEL PERFORMANCE

Calibration of the test tunnel included the establishment of heat flux and total enthalpy throughout the test section. Pertinent data are presented in Figures 5 and 6.

Tunnel stagnation performance data are presented in Table II. These values are gas flow, power input, plenum chamber pressure, nozzle exit pressure, stagnation pressure, and stagnation heat transfer rates to the test models. Analysis of these data shows that the tunnel repeated the desired stagnation heat transfer rate throughout the test series with a maximum deviation from the mean of 1.68 percent. Analysis of ablation rate and effective heat of ablation data indicate a maximum deviation from the mean of 8.4 percent.

Table IV shows the heat flux to model sides as determined by transient calorimetry.

SUMMARY OF MEASUREMENTS

All numerical test data derived from measurements made throughout this test program are presented in Tables I through V. Time temperature trace curves are presented in the Illustrations sections of this report.

TABLE I

TEST SCHEDULE

Model No.	Material	Coating Thickness (in.)		Test Condition*
		Side Wall	Stag. Point	
Cal. 6	Cu. Body	-	-	1
1A	T-500	.006	1.247	1
2B	T-500	.010	1.251	1
3C	T-500	.015	1.252	1
4D	T-500	.020	1.251	1
5B	Phen. N.	.012	1.249	1
6D	Phen. N.	.020	1.253	1
7E	Phen. N.	.027	1.250	1
8F	Phen. N.	.035	1.253	1
Cal.4	Cu. Body	-	-	2
9B	T-500	.010	1.251	2
10D	T-500	.020	1.249	2
18A	T-500	.005	1.253	2
11E	T-500	.030	1.252	2
13D	Phen. N.	.017	1.256	2
14F	Phen. N.	.034	1.255	2
17B	Phen. N.	.011	1.250	2
15G	Phen. N.	.051	1.250	2

*Condition #1: h_t = 3500 BTU/lb, q_m = 33 BTU/ft^2- sec
Condition #2: h_t = 17,500 BTU/lb, q_m = 333 BTU/ft^2-sec

TABLE II
TEST CONDITIONS

	Model No.	Power Input (Kw)	Power in Gas (Kw)	Mass Flow (lb/sec)			h_t - (BTU/lb)	P_t (atm.)	P'_o (atm.)	P_o (atm.)	Mach No.	q_c (BTU/ft^2-sec)	q_m (BTU/ft^2-sec)	Deviation of q_m from mean value
				N_2	O_2	Total								
Test Condition #1	Cal. 6	28.84	8.88	.001896	.000504	.00240	3510	.0418	.0098	.00875	3.0	78.2		
	1A	29.05	8.88	.001896	.000504	.00240	3510	.0420	.0098	.00880	3.0	77.8	30.03	+.74%
	2B	29.10	9.11	.001896	.000504	.00240	3600	.0423	.0097	.00879	3.0	77.0	30.16	+1.17%
	3C	29.00	9.98	.001896	.000504	.00240	3550	.0420	.0099	.00890	3.0	77.7	30.31	+1.68%
	4D	29.00	9.14	.001896	.000504	.00240	3610	.0420	.0099	.00880	3.0	77.0	30.18	+1.24%
	5B	28.35	9.33	.001896	.000504	.00240	3685	.0409	.0095	.00890	3.0	77.5	29.82	-.97%
	6D	28.25	9.11	.001896	.000504	.00240	3598	.0419	.0098	.00878	3.0	76.9	29.32	-1.66%
	7E	28.35	9.06	.001896	.000504	.00240	3580	.0419	.0098	.00890	3.0	76.8	29.36	-1.51%
	8F	28.57	9.05	.001896	.000504	.00240	3575	.0419	.0098	.00879	3.0	76.8	29.59	-.74%
Test Condition #2	Cal. 4	130.6	63.8	.002765	.000735	.00350	17,450	.1040	.0188	.00191	3.0	782.0		
	9B	128.5	64.78	.002765	.000735	.00350	17,550	.1038	.0189	.00190	3.0	779.8	360.6	+.75%
	10D	129.1	64.50	.002765	.000735	.00350	17,475	.1042	.0188	.00189	3.0	783.5	362.8	
	18A	129.2	64.46	.002675	.000735	.00350	17,465	.1041	.0189	.00191	3.0	785.5	362.8	+1.38%
	11E	129.2	64.91	.002765	.000735	.00350	17,585	.1041	.0189	.00190	3.0	784.5		
	13D	129.5	64.52	.002765	.000735	.00350	17,480	.1040	.0188	.00191	3.0	785.0	358.6	-.64%
	14F	128.0	64.83	.002765	.000735	.00350	17,565	.1040	.0189	.00191	3.0	782.4	354.7	-.89%
	17B	130.0	64.59	.002765	.000735	.00350	17,500	.1040	.0188	.00190	3.0	784.3	354.5	-.95%
	15G	128.8	64.18	.002765	.000735	.00350	17,389	.1040	.0188	.00191	3.0	783.8	354.3	-1.00%

TABLE III
MATERIAL DENSITIES

Material	Average Measured Density (lb/ft^3)
Phenolic Nylon	42.6
T-500, Molded	80.0
T-500, Sprayed	72.0
Phenolic Nylon (Char Layer)	14.14
T-500 (Debris Layer) Surface	32.0
Middle of debris	17.7

TABLE IV
CALORIMETER RESULTS

	Time (sec)	Sidewall Heat Flux BTU/ft^2 sec
Hemisphere Cylinder Calorimeter #6 Total Enthalpy = 3510 BTU/lb Heat Flux to 5/8" Diameter Calorimeter = 78.2 BTU/ft^2-sec	2	.6
	8	1.4
	14	2.8
	24	3.5
	34	3.9
	40	4.0
	44	3.9
	Value	= 4.0 BTU/ft^2 sec
Hemisphere Cylinder Calorimeter # 4 Total Enthalpy = 17,450 BTU/lb Heat Flux to 5/8" Diameter Calorimeter = 780.2 BTU/ft^2-sec	7.5	58
	15	64
	23	67
	30	79
	Average Value	67 BTU/ft^2sec

TABLE V

STAGNATION POINT RESULTS

	Model Number	Material	Test Duration (Min.)	Weight Change (gm.)	Total Enthalpy (BTU lb.)	Recession to Debris (in.)	Debris Thickness (in.)	Total Recession (in.)	Hot-Wall Heat Flux (BTU/ft^2-sec)	Surface Temperature (°F.)	Hot-Wall Heat Blockage (BTU lb*)
Test Condition # 1	1A	T-500	16.7	51.70	3510	0.054	.470	.524	31.20	2550	8930
	2B	T-500	16.7	49.10	3600	0.065	.435	.500	31.50	2445	9450
	3C	T-500	12.7	51.50	3550	-	.340	.340	31.65	2445	10.530
	4D	T-500	12.7	47.80	3610	-	.365	.365	31.75	2445	9950
	5B	Phen. N.	16.7	70.70	3685	1.176	-	-	30.48	2800	4660
	6D	Phen. N.	16.7	70.30	3598	1.108	-	-	30.05	2800	4300
	7E	Phen. N.	16.7	72.10	3580	0.854	-	-	30.32	2695	4630
	8F	Phen. N.	16.7	70.40	3575	1.023	-	-	30.40	2695	4320
Test Condition # 2	9B	T-500	5.0	52.90	17,550	0.593	.055	.648	363.90	3900	14,600
	10D	T-500	5.0	48.80	17,475	0.605	.065	.670	366.00	3900	14,300
	18A	T-500	5.0	51.25	17,465	0.631	.050	.681	367.00	3900	13,950
	11E	T-500	11.0	101.10	17,585	-	.100	-	365.50	3950	13,450
	13D	Phen. N.	5.0	40.30	17,460	0.895	.285	1.180	361.50	4270	10,470
	14F	Phen. N.	5.0	41.35	17,565	0.923	.295	1.218	360.00	4220	10,090
	17B	Phen. N.	5.0	45.75	17,500	0.871	.285	1.156	361.50	4270	10,600
	15G	Phen. N.	5.0	43.50	17,389	0.934	.265	1.199	360.00	4270	10,160

* Hot-Wall heat blockage results for test Condition #1 are uncorrected for radiation; the Hot-Wall heat blockage results for test Condition #2 are corrected for radiation.

DISCUSSION OF RESULTS

MATERIAL PERFORMANCE ON SIDE WALLS.

TEST CONDITION #1.

Material performance at Test Condition #1 (enthalpy 3500 BTU/lb, heat flux 4 BTU/ft^2 sec) is described in the following paragraphs.

"THERMO-LAG" T-500. Four "THERMO-LAG" T-500 models of different coating thicknesses were tested. The model numbers, coating thicknesses, coating weights, and test durations are shown in Table VI.

TABLE VI

Model Number	Coating Thickness (in.)	Coating Weight (lb/ft^2)	Test Duration (min)
1A	.006	.036	16.67
2B	.010	.060	16.67
3C	.015	.090	12.5
4D	.020	.120	13.

MODEL 1A: Figure 14 contains profile and sectional views of the model. It will be noted that the model maintained its original configuration throughout the test. Figure 16 contains the thermocouple temperature traces obtained at thermocouple locations 2 and 3 on the steel substrate. Thermocouple trace #2 shows a higher temperature than thermocouple trace #3 throughout the test, indicating either a thermocouple calibration error or a slight misalignment of the model. To present the data in the material comparison curves (q^{**} versus T) an average temperature representing the arithmetic mean of the two thermocouples temperatures was used. The steel cylinder temperature became asymptotic to the sublimation temperature (530°F) of the "THERMO-LAG" T-500 after ten minutes.

Post-test microscopic inspection of the model indicated that most of the salt had sublimed away, and only the debris layer, composed of the binder system and certain additives, remained over the thermocouples.

MODEL 2B: Figure 18 depicts the model, at Test Condition #1, before and after a test of 16.67 minutes. This illustration shows that the model maintained its original configuration throughout this test. Figure 20 contains the thermocouple temperature traces obtained at thermocouple locations 2 and 3 on the steel substrate. The temperatures are lower than the other temperature test data. The temperature of the substrate became

asymptotic to 300°F. Post-test microscopic inspection of the model indicated that very little of the salt in the virgin "THERMO-LAG" T-500 had sublimed. These data results are not consistent with the other measurements. Possible explanations for this inconsistency include faulty calibration of instrumentation, drifting of the instrumentation, and varying instrumentation power supply. These data have been reduced in terms of q^{**} versus T and plotted as dotted lines on Figure 48.

MODEL 3C: Figure 22 depicts the model before and after a 12.5-minute test. This illustration shows that the model maintained its original configuration throughout the test. After the model had been exposed to plasma jet for five minutes, the sting support failed and the model assumed a $\simeq 3°$ angle in the plasma stream. The sting assembly failed completely at 12.5 minutes, causing termination of the test. Figure 24 presents the thermocouple temperature traces obtained from the steel cylinder. These thermocouple temperature traces are similar to the other traces obtained during this test series pertaining to asymptotic behavior. After the failure of the sting assembly, which occurred after five minutes of testing, the temperatures rose to 660°F. The test was terminated at this point. Post-test microscopic inspection of the model revealed that most of the salt had sublimed away from the side of the model stagnant to the stream, and that the binder system had started to pyrolyze. Figure 49 shows the plot of these data presented in terms of q^{**} versus T. The period of testing preceding sting failure is shown by solid lines, the period after sting failure is not shown.

MODEL 4D: Figure 26 depicts the model before and after a 13 minute test. This figure shows that the model retained its original configuration throughout the test, although the sting assembly failed after nine minutes of the test, causing the model to become misaligned in the plasma jet. Due to the failure of the sting assembly, no valid data was obtained after nine minutes of this test. Figure 28 presents the temperature traces of the skin thermocouples. These traces are asymptotic to 530°F. Inspection of the model indicated that most of the salt had sublimed from the side of the model stagnant to the stream, and that the binder had begun to pyrolyze. Figure 50 presents the plot of these data presented in terms of q^{**} versus T for the nine minute test period.

The performance of "THERMO-LAG" T-500 at Test Condition #1 indicated that:

1. A nonreceding char layer was formed and the models retained their original configuration throughout the test.
2. Approximately .005 to .006 inch of virgin "THERMO-LAG" T-500 was consumed in a 16.67 minute test period.
3. The sprayed coating of "THERMO-LAG" T-500 adhered to the steel skin throughout the test.
4. The temperature of the steel skin when protected with "THERMO-LAG" T-500 asymptotically approached 530°F, the subliming temperature of "THERMO-LAG" T-500.
5. After the salt had sublimed from the virgin "THERMO-LAG" T-500, the binder system began to pyrolyze, and afforded additional thermal protection.

PHENOLIC NYLON. Four low-density phenolic nylon models with different thicknesses of coating were tested at Test Condition #1 (enthalpy 3500 BTU lb, heat flux 4 BTU ft^2 sec). The model numbers and coating thicknesses, coating weights, and test durations are shown in Table VII.

TABLE VII

Model No.	Coating Thickness (in.)	Coating Weight (lb ft^2)	Test Duration (min)
5B	.012	.0425	16.7
6D	.020	.071	16.7
7E	.027	.096	16.7
8F	.035	.125	16.7

MODEL 5B: Figure 15 depicts the model before and after a 16.67 minute test. Figure 17 contains the thermocouple temperature traces obtained at thermocouple locations 2 and 3 on the steel substrate. During this test of the phenolic nylon model, the hemispherical stagnation region changed from its normal shape to an irregular, cupped configuration. This change in configuration caused an observable, discontinuously stepped change in the flow field about the model. After two minutes of testing, the flow field separated from the afterbody of the model, terminating the further acquisition of valid data. The visual observation of the flow field separation coincided with the erratic thermocouple traces. The temperature rose steadily from the three-minute point to the end of the test. Maximum temperature attained was approximately 860°F. No positive temperature control characteristics of this ablating material could be determined from this test. Figure 47 presents the reduced data in terms of q^{**} versus T. Data acquired during the first two minutes of test is represented by solid lines. Data acquired after two minutes of testing has been deleted due to its limited validity. The substrate temperature, T, is taken as the mean temperature of thermocouples 2 and 3.

The model was left in the plasma jet for 16.67 minutes. The stagnation region completely ablated, and the material around the leading periphery of the cylinder was consumed. The ablation around the cylinder was irregular. The irregularity of ablation, together with the variance in indicated thermocouple temperatures indicates that the model was slightly misaligned in the stream. It was noted that cracks had developed in the coating over the aft portion of the cylinder.

Due to the erratic behavior of the flow field, valid material ablation criteria were not established during this test after the two minute exposure. Post-test microscopic inspection of the char layer in the region of thermocouple 2 revealed that all of the nylon had ablated, leaving only the char layer. A similar inspection at thermocouple 3 revealed that while a char layer had started to form, nylon was still visible in the material.

MODEL 6D: Figure 19 depicts the model before and after a 16.67-minute test period. Figure 21 contains the thermocouple temperature traces obtained at thermocouple locations 2 and 3.

During this test, the shape of the phenolic nylon model changed from a hemispherical cylinder to an irregular cup-shaped configuration. This peculiar configuration caused the flow field to separate from the afterbody of the model after two minutes of testing. The visual observation of the flow field separation again coincided with recorded thermocouple temperature traces. These temperature traces became erratic after two minutes of testing, and after four minutes of testing, the substrate temperature increased steadily until the end of the test. At this time the substrate temperature had reached 800°F. No positive temperature control characteristics of this ablative material could be determined from this test.

Figure 48 presents the reduced data in terms of q^{**} versus T. Solid lines indicate the plot of the data for the first two minutes of test, while data of limited validity which was acquired after this time has been deleted. The substrate temperature, T, is taken as the mean temperature of thermocouples 2 and 3 at any given time.

No valid criteria regarding material ablation were established during this test because of the erratic nature of the flow field caused by nonuniform ablation.

Following this test, the char layer in the regions of thermocouples 2 and 3 was subjected to microscopic examination. It was observed that although a char layer had started to form at thermocouple 2, nylon was still visible in the material, while at thermocouple 3 all of the nylon was gone and only the char layer remained.

Misalignment of the model in the plasma jet stream was indicated by the peculiar way in which the material ablated, and by the characteristics of the thermocouple traces.

MODEL 7E: Figure 23 depicts the model before and after the 16.67-minute test. Figure 25 contains the thermocouple temperature traces obtained at thermocouple locations 2 and 3 on the steel substrate.

During this test, the shape of the phenolic nylon model assumed an irregular, cup-shaped configuration, causing the flow field to separate from the afterbody of the model after two minutes of testing. Visual observation of flow field separation coincided with thermocouple temperature trace indications which became erratic after two minutes of testing. Thermocouple 3 failed completely after three minutes of testing, while after seven minutes of testing, thermocouple 2 indicated a rise in temperature to a maximum of 700°F.

Figure 49 presents the reduced substrate temperature data in terms of q^{**} versus T. Solid lines indicate the plot of the data for the first two minutes of test. Data of limited validity acquired after this time has been deleted. The substrate temperature, T, is taken as the temperature of thermocouple 2 for this test.

No valid criteria regarding material ablation were established during this test because of the erratic nature of the flow field caused by nonuniform ablation. Following this test, microscopic examination revealed that the material over both thermocouples 2 and 3 was somewhat charred, although phenolic nylon was still visible in the virgin material, and nylon bubbles were visible over the side of the model in the test area.

MODEL 8F: Figure 27 depicts the model before and after a 16.67-minute test. Figure 29 contains the thermocouple temperature traces obtained at thermocouple locations 2 and 3 on the steel substrate. During this test, the stagnation region of the phenolic nylon model changed from a hemispherical to an irregular, cup-shaped configuration, causing an observable, discontinuously stepped change in the flow field. After two minutes of testing the flow field separated from the afterbody of the model, rendering invalid the data acquired after this time. Visual observation of flow field separation coincided with thermocouple temperature trace indications which became erratic after two minutes.

Following the flow field separation at two minutes of testing, the thermocouple temperature traces indicated a decrease in the temperature of the steel substrate. The decrease in temperature continued until ten minutes, when the temperature began to rise, attaining a maximum of 600°F at the termination of this test.

No positive temperature control characteristics of this ablative material could be determined from this test.

Figure 50 presents the reduced substrate temperature data in terms of q^{**} versus T. Solid lines indicate the plot of data for the first two minutes of test. Data of limited validity acquired after two minutes of testing has been deleted.

The substrate temperature, T, is taken as the mean temperature of thermocouples 2 and 3.

No valid criteria regarding material ablation were established during this test because of the erratic nature of the flow field caused by nonuniform ablation.

Microscopic examination of the regions of thermocouples 2 and 3 revealed that nylon was still present in the phenolic matrix although charring was noted. Nylon bubbles were present over the entire surface of the model.

The performance of phenolic nylon at Test Condition #1 indicated that:

1. The stagnation region of the phenolic nylon ablated rapidly, causing the flow field about the test section to change in a discontinuous fashion and to separate from the model surface after two minutes of testing. Therefore, the results of the remaining part of the test were invalidated.
2. The adhesive used to attach the phenolic nylon to the steel surface held up well throughout the test.
3. No positive temperature control characteristics, temperature of melting or degradation of the phenolic nylon could be determined from this series of tests.

TEST CONDITION #2.

Material performance at Test Condition #2 (stagnation enthalpy 17,500 BTU/lb, heat flux 67 BTU ft^2 sec) is described in the following paragraphs.

"THERMO-LAG" T-500. Four "THERMO-LAG" T-500 models of different coating thicknesses were tested. The model numbers, coating thicknesses, coating weights, and test durations are shown in Table VIII.

TABLE VIII

Model No.	Coating Thickness (in.)	Coating Weight (lb/ft^2)	Test Duration (min)
9B	.010	.06	5
10D	.020	.12	5
18A	.005	.03	5
11E	.030	.180	11

MODEL 9B: Figure 30 depicts the model before and after a five-minute test. Figure 32 contains the thermocouple temperature traces obtained at thermocouples 2 and 3 on the steel substrate. During this test the surface of the model receded and flattened rapidly, causing the flow field to go through an observable, discontinuous step change. After approximately 1-1/2 minutes of testing the flow field separated from the cylindrical afterbody of the model.

Uneven ablation of the material in the stagnation region indicated that the model was misaligned in the plasma jet stream.

Erratic thermocouple traces indicated a rise in temperature to 800°F, followed by a decay to 530°F. Comparison of these inconsistent temperature data to the rest of the test data causes them to be considered invalid, and they are not included in the material comparison study.

Criteria of mass loss could not be established because of the separation of the flow field.

Microscopic examination of the model following the test failed to reveal any salt in the region of either thermocouple. Although the coating adhered well to the steel substrate, the binder system had begun to pyrolze.

MODEL 10D: Figure 34 depicts the model before and after a five-minute test. Slight misalignment of the model during this test is indicated by the rapid receding and flattening of the model surface. This change in configuration caused the flow field to go through an observable, discontinuous change and to separate from the afterbody of the model after 1-1/2 minutes of testing.

Figure 51 presents the reduced substrate temperature of terms of q^{**} versus T, where the temperature of the steel substrate is taken as the mean of thermocouples 2 and 3 at any given time. Solid lines indicate the plot of data for the initial 1-1/2 minutes of testing (until flow field separation). Dotted lines indicate data of limited validity.

Figure 36 contains the thermocouple traces. These thermocouple temperature traces indicate an attained maximum temperature of 450°F, thus demonstrating the positive temperature control characteristics of "THERMO-LAG" T-500.

Microscopic examination of the model following the test indicated that although some of the salt had sublimed, the coating had adhered to the steel substrate during the test. The amount of salt remaining in the material was not determined.

MODEL 18A: Figure 38 depicts the model before and after a five-minute test. Slight misalignment of the model in the plasma jet stream is indicated by rapid receding and flattening of the model surface in the stagnation region. This change in configuration caused the flow field to go through an observable, discontinuous change, and to separate from the afterbody of the model after 1-1/2 minutes of testing.

Figure 40 contains the thermocouple temperature traces which indicate asymptotic behavior of the steel substrate temperature approaching the sublimation temperature of "THERMO-LAG" T-500. Maximum temperature recorded during this test was 440°F.

Figure 52 presents the valid data for the first 1-1/2 minutes of testing, in terms of q^{**} versus T, where the temperature of the steel substrate is taken as the mean of thermocouples 2 and 3 at any given time. The data up to flow field separation are plotted in solid lines, the data of limited validity are plotted in dotted lines.

Microscopic examination of the model following test completion revealed that the sprayed on coating adhered to the steel substrate throughout the test, and also that some of the salt had sublimed. The exact amount was not determined.

MODEL 11E: Figure 42 depicts the model before and after an 11-minute test. The stagnation region of the surface receded and flattened rapidly, causing the flow field to go through an observable discontinuous change after 1-1/2 minutes of testing. The thermocouple traces are presented in Figure 44. The temperature traces indicate asymptotic

behavior of the steel substrate temperature approaching the sublimation temperature of "THERMO-LAG" T-500. The maximum temperature recorded during this test was 490°F. These data are considered valid for the first 1-1/2 minutes of testing and are presented in Figure 53 in terms of q^{**} versus $\bar{T}$, where the temperature of the steel substrate is taken as the means of thermocouples 2 and 3 at any given time. The data up to 1-1/2 minutes of testing, the time of flow field separation, is plotted in solid lines, while the data of limited validity are indicated by dotted lines.

Microscopic examination of the model following test completion indicated that the sprayed on coating adhered to the steel substrate throughout an 11-minute test, and although some of salt had sublimed, the exact amount was not determined.

The performance of "THERMO-LAG" T-500 at Test Condition #2 indicated that:

1. .005 inch of "THERMO-LAG" T-500 maintained thermal protection of the steel substrate holding the temperature below 500°F for 5 minutes.
2. .030 inch of "THERMO-LAG" T-500 maintained the temperature of the steel substrate below 500°F for 11 minutes.
3. The sprayed on coating of "THERMO-LAG" T-500 adhered to the steel cylinder for periods of up to 11 minutes without any indications of failure.
4. In all tests, the "THERMO-LAG" T-500 maintained the temperature of the steel substrate below 530°F.

PHENOLIC NYLON. Four phenolic nylon test models with different coating thicknesses were run at Test Condition #2. The model numbers, coating thicknesses, coating weights, and test durations are shown in Table IX.

TABLE IX

Model Number	Coating Thickness (in.)	Coating Weight (lb/ft^2)	Test Durations (min)
13D	.017	.06	5
14F	.034	.12	5
17B	.011	.0385	5
15G	.051	.182	5

MODEL 13D: Figure 31 depicts the model before and after a 5-minute test. The photographs indicate slight misalignment of the model in the plasma jet during the test. The stagnation region receded and flattened rapidly, causing the flow field to go through an observable discontinuous change and separate from the afterbody after 2 minutes of testing.

The thermocouple traces are presented in Figure 33. The thermocouple temperature rose throughout the test and was asymptotic to some value. The maximum temperature attained was 630°F. The data are considered valid for the first two minutes of the test.

Microscopic examination of the model following completion of the test revealed the following:

1. A crack occurred at the aft end of the model, and the coating had separated from the steel substrate.
2. Nylon had flowed out of the phenolic matrix and formed bubbles.
3. The material had discolored and had begun to form a char layer. Accurate measurement of the total material consumed was not made.

MODEL 14F: Figure 35 depicts the model before and after a 5 minute test. Slight misalignment of the model in the plasma jet during the test is indicated. The stagnation region of the model receded and flattened rapidly, causing the flow field to go through an observable, discontinuous change and separate from the afterbody of the model after 1-1/2 minutes of testing.

Figure 37 contains the thermocouple temperature traces. The temperature increased steadily during the test, and was asymptotically approaching its limiting value of 900°F. The maximum temperature attained during this test was 660°F.

Figure 51 presents the data, considered valid for the initial 1-1/2 minutes of testing, in terms of q^{**} versus T. The temperature of the steel substrate is taken as the mean of thermocouples 2 and 3 at any given time.

The data acquired prior to flow field separation is plotted in solid lines and the data of limited validity is indicated by dotted lines. Microscopic examination of the model following test completion revealed that the nylon had flowed out of the phenolic matrix and had formed bubbles along the side of the model. The material had discolored and had started to form a char layer.

MODEL 17B. Figure 39 depicts the model before and after 5 minutes of testing. The slight misalignment of the model in the plasma jet during the test is indicated. The stagnation region receded and flattened rapidly, causing the flow field to go through an observable, discontinuous change, and separate from the afterbody of the model after 1-1/2-minute of testing.

Figure 41 contains the thermocouple traces. The steel substrate temperature increased throughout the test and was asymptotically approaching 900°F. The maximum temperature attained was 890°F.

Figure 52 presents the data considered valid for the first 1-1/2 minute of the test. The data is presented in terms of q^{**} versus T. The temperature of the steel substrate is taken as the mean of thermocouples 2 and 3 at any given time. The data up to the time of flow field separation is plotted in solid lines, while the data of limited validity is indicated by dotted lines.

Microscopic examination of the model following test completion indicated that the coating had failed completely and separated from the steel substrate over thermocouple 3. The coating over thermocouple 2, although charred, had adhered well.

MODEL 15G: Figure 43 depicts the model before and after a 5 minute test. The stagnation region of the model receded and flattened rapidly, causing the flow field to go through an observable, discontinuous change, and separate from the afterbody of the model after 1-1/2 minutes of testing.

Figure 45 contains the thermocouple traces. The steel substrate temperature increased throughout the test, and attained a maximum temperature of 835°F at the end of the test. Figure 53 presents the data, which is considered valid for the initial 1-1/2 minutes of testing. The data is presented in terms of q^{**} versus T, where the temperature of the steel substrate is taken as the mean of thermocouples 2 and 3 at any given time. The data, up to the time of flow field separation, is plotted in solid lines, while data of limited validity is indicated by dotted lines.

Microscopic examination of the model following test completion revealed that the phenolic nylon had cracked and lost bond over thermocouple 3, and had flowed out of the phenolic matrix and formed bubbles on the side of the model. It was also observed that the material had discolored and started forming a char layer. Accurate measurements of the total material consumed were not made.

The phenolic-nylon performance at Test Condition #2 indicated that:

1. The phenolic-nylon offered thermal protection and maintained the substrate temperatures below 900°F, but not enough data was obtained to accurately establish the degradation temperature.
2. One of the better high temperature adhesives (Epoxylite) started failing after five minutes of testing.
3. The phenolic nylon cracked and had a tendency to spall.

COMPARISON OF MATERIAL PERFORMANCES WHEN APPLIED IN THIN COATINGS ON SIDE WALLS.

Figures 48 through 53 contain the results of the tests which are plotted in terms of q^{**} versus T, where q^{**} is $q \frac{\text{average x time and}}{\text{mass of coating}}$ T is the steel substrate temperature. The figures directly compare the substrate temperature histories for approximately equal

coating weight per unit area in identical thermal environments. The flow field about the model was a strong function of the forebody geometry. When the stagnation region ablated and flattened, the flow field underwent an observable, discontinuous change, and separated from the model afterbody, thus reducing the heat transfer rate in the test section. Due to model forebody shape change, the test data for phenolic nylon at Test Condition #1 was valid for the first two minutes of the test. The "THERMO-LAG" T-500 at Test Condition #1 formed a nonreceding debris layer and the data are valid throughout the test. At Test Condition #2, the "THERMO-LAG" T-500 underwent a flow field discontinuity at 2 minutes, and the phenolic nylon test had a flow field discontinuity at 1-1 2 minutes. The test data are completely valid only up to the time of flow field discontinuity, however the performance comparisons may be extended for the five minutes of test.

The comparison of the performance of "THERMO-LAG" T-500 and phenolic nylon in thin-coat applications on side walls is summarized in the following table.

TABLE X

"THERMO-LAG" T-500			Phenolic Nylon		
Test Condition	Coating Thickness	Temperature	Coating Thickness	Temperature	Data Compares Figure No.
1	.036	325°F*	.0425	390°F*	15 and 23
1	.060	200°F*	.071	500°F*	17 and 25
1	.090	360°F*	.096	590°F*	19 and 27
1	.120	310°F*	.125	520°F*	21 and 29
2	.03	430**	.0385	880**	35 and 43
2	.06	—	.06	590**	31 and 39
2	.12	430**	.12	620**	33 and 41
2	.180	440**	.182	770**	37 and 45

* indicates temperature after two minutes.
** indicates maximum temperature.

In all cases the "THERMO-LAG" T-500 maintained the steel substrate temperature below the sublimation temperature of 530°F. The phenolic nylon maintained the steel substrate below 900°F, which is apparently the melting and degradation temperature of phenolic nylon.

In all cases the "THERMO-LAG" T-500 was more efficient than phenolic nylon when used in thin coatings as a thermal protection system at low heat flux levels.

The phenolic nylon coating attached to the steel with epoxylite showed signs of cracking after a five-minute test. In all tests the nylon melted, started flowing out of the phenolic matrix, and formed bubbles. The "THERMO-LAG" T-500 sprayed directly over the steel substrate adhered throughout all tests for the maximum test periods of 11 and 16.67 minutes.

MATERIAL PERFORMANCE AT THE STAGNATION REGION.

TEST CONDITION #1.

Material performance at test condition #1 (enthalpy 3500 BTU/lb, heat flux 30 BTU/ft^2 sec) is described in the following paragraphs.

"THERMO-LAG" T-500. Four "THERMO-LAG" T-500 models were tested at Test Condition #1. The results are shown in Table XI.

TABLE XI

Model No.	Test Duration (min)	Recession to Debris (in.)	Debris Thickness (in.)	Virgin Material Recession (in.)	Stagnation Heat Flux (BTU/ft^2 sec)	Surface Temperature (°F)	Gross Heat Blockage (BTU/lb)
1A	16.7	.054	.470	.524	31.2	2550	8930
2B	16.7	.065	.435	.500	31.5	2445	9450
3C	12.6	—	.340	.340	31.7	2445	10,530
4D	12.7	—	.365	.365	31.8	2445	9950

1. The surface temperatures were measured with an optical pyrometer at approximately 1/2-minute intervals. The results are presented in Figure 10 for all models. The average surface temperature was 2470°F.

2. The temperature histories of the copper plugs 1-1/4 inches from the original model surface are plotted in Figure 10. The temperature attained a maximum of 250°F.
3. The average gross heat blockage for the four models is 9715 BTU/lb. The data are presented in Figure 46.
4. The four models performed similarly and had identical physical appearance after removal from the plasma jet stream. Post-test analysis of the models included axial sectioning. Views of the sectioned models are shown in Figures 14, 18, 22, and 26.

The debris layer receded approximately .06 inch and then formed a stable nonreceding surface capable of obtaining a high surface temperature. The models retained the hemispherical cylinder configuration throughout the test. The sectioned debris had: (a) microscopically thin light-colored hard crust; (b) beneath the crust a large pore "char" structure .250 inch thick with "char" cells approximately .02 inch in diameter; and (c) a sharp line of demarcation where the debris matrix was a lighter color for .220 inch down to the surface of the virgin material.

PHENOLIC NYLON. Four phenolic nylon models were tested at Test Condition #1. The results are shown in Table XII.

TABLE XII

Model No.	Total Test Duration (min)	Recession to Char (in.)	Time for Recession to Calorimeter 1-1/4 in. from Stag. Pt.	Virgin Material Recession (in.)	Stagnation Heat Flux (BTU/ft^2sec)	Surface Temperature (°F)	Gross Heat Blockage (BTU/lb)
5B	16.7	1.176	11.3		30.5	2800	4660
6D	16.7	1.108	10.6		30.1	2800	4300
7E	16.7	.854	11.3		30.3	2695	4630
8F	16.7	1.023	10.5		30.4	2695	4320

1. The surface temperatures were measured with an optical pyrometer at approximately 1/2-minute intervals. The results are presented in Figure 11 for all models. The average surface temperature attained was 2748°F.

2. The temperature histories of the copper plugs 1-1/4 inches from the original model surface are plotted in Figure 11 for all models.

The stagnation region thermocouple showed a peculiar response at 1-1/2 to 2-1/2 minutes, which occurred at the same time the flow field went through the dissociative change. This effect is not explained herein.

3. The average gross heat blockage for the four models is 4477 BTU/lb. The data are presented in Figure 46.
4. The four models performed similarly and had identical physical appearance, after removal from the plasma jet stream. All models had receded rapidly and changed from a hemispherical cylinder to an irregular, cup-shaped configuration. There was not enough stagnation region char left to allow the models to be sectioned.

TEST CONDITION #2.

Material performance at Test Condition #2 (enthalpy 17,500 BTU/lb, heat flux 360 BTU/ft^2 sec) is described in the following paragraphs.

"THERMO-LAG" T-500. Four "THERMO-LAG" T-500 models were tested at Test Condition #2. The results are shown in Table XIII.

TABLE XIII

Model No.	Test Duration (min)	Recession to Debris (in.)	Debris Thickness (in.)	Total Recession (in.)	Stagnation Heat Flux (BTU/ft^2 sec)	Surface Temperature (°F)	Heat Blockage $\frac{q_m}{\dot{m}}$ (BTU/lb)	Heat Blockage $\frac{q_m - q_r}{\dot{m}}$ (BTU/lb)
9B	5	.593	.055	.648	363.9	3900	25,300	14,600
10D	5	.605	.065	.670	366.0	3900	24,600	14,300
18A	5	.631	.050	.681	367.0	3900	24,300	13,950
11E	11	——	.100	——	365.5	3950	23,200	13,450

1. The surface temperatures were measured with an optical pyrometer at approximately 1/2-minute interval. The results are presented in Figure 12 for all models. The average surface temperature was 3912°F.

2. The temperature histories of the copper plugs 1-1/4 inches from the original model stagnation point are plotted in Figure 12. Models 9B, 10D and 18A were exposed for five minutes to the plasma jet, the temperatures were recorded for eight minutes to establish model "cooling curves". The maximum temperature attained by these models was 170°F.

   Model 11E was exposed for 11 minutes to the plasma jet stream. After 8.2 minutes the temperature started rising rapidly. To achieve consistency with all data, the "THERMO-LAG" T-500 was considered all consumed when the copper slug reached 500°F, which occurred at 8.84 minutes.

3. The average gross heat blockage was 24,350 BTU/lb. The endothermic decomposition, latent heat of sublimation, and transpiration cooling $\frac{q_m - q_r}{\dot{m}}$ was 14,075 BTU/lb. These data are presented in Figure 46.
4. Models 9B, 10D and 18A receded an average of 0.666 inch. They performed similarly and had identical physical appearance. The stagnation region was sectioned axially. Figures 30, 34, 38 and 42 are photographs of the sectioned models. The debris matrix was thin (.06 inch), black and uniform and had a fine microscopic pore structure, as shown in Figure 55.

   Model 11E was tested for 11 minutes. The stagnation region had cupped and receded past the copper calorimeter.

PHENOLIC NYLON. Four phenolic nylon models were tested at Test Condition #2. The results are shown in Table XIV.

TABLE XIV

Model No.	Test Duration (min)	Recession to Char. (in.)	Char Thickness (in.)	Total Recession (in.)	Stagnation Heat Flux (BTU/ft² sec)	Surface Temperature (°F)	Heat Blockage $\frac{q_m}{\dot{m}}$ (BTU/lb)	Heat Blockage $\frac{q_m - q_r}{\dot{m}}$ (BTU/lb)
13D	5	.895	.285	1.180	361.5	4270	25,800	10,470
14F	5	.923	.295	1.218	360.0	4220	25,000	10,090
17B	5	.871	.285	1.156	361.5	4270	26,300	10,600
15G	5	.934	.265	1.199	360.0	4270	25,200	10,160

1. The surface temperatures were measured with an optical pyrometer at approximately 1/2-minute intervals. The results are presented in Figure 13 for all models. The average surface temperature was 4258°F.
2. The temperature histories of the copper plug 1-1/4 inches from the stagnation point are shown in Figure 13. The copper plug recorded a maximum of 380°F which occurred 30 seconds after termination of the test.
3. The average gross heat of ablation was 25,575 BTU/lb. The energy of degradation and transpiration cooling $\left(\frac{q_m - q_r}{\dot{m}}\right)$ was 10,330 BTU/lb. The data are presented in Figure 46.
4. The models all performed similarly and receded an average of 1.188 inches during the five-minute test. All four models had similar physical appearance. After the test the models were sectioned axially. Photographs of the sectioned model are presented in Figures 31, 35, 39 and 43. The phenolic char was down to the reaction zone and the surface of the virgin material. The char was approximately .290 inch thick and was a coarse porous structure with "char" cells approximately .05 inch in diameter.

COMPARISON OF MATERIAL PERFORMANCE AT THE STAGNATION REGION.

The performance comparison data for "THERMO-LAG" T-500 and low-density phenolic nylon at the stagnation point are presented in Figure 46. The total effective heat blockage $\frac{q_m - q_r}{\dot{m}}$ is plotted versus total enthalpy in Figure 46. The data are connected by dotted lines to indicate trends. No effective comparison of materials was made at the stagnation point using a backside temperature rise as the criterion.

The "THERMO-LAG" T-500 at Test Condition #1 formed a nonconsumable debris matrix capable of reaching radiation equilibrium temperature. Phenolic nylon receded rapidly at Test Condition #1 and was relatively ineffective as a thermal protection system.

The effect of endothermic reactions and mass injection was compared by plotting $\frac{q_m - q_r}{\dot{m}}$ versus total stream enthalpy as presented in Figure 46 where data points have been obtained from other sources, only to help establish trends. The data indicate that "THERMO-LAG" T-500 undergoes 3745 BTU/lb more endothermic reaction and mass injection effects than phenolic nylon at Test Condition #2. The performance of "THERMO-LAG" at high heat flux levels is attributable primarily to mass injection and endothermic reactions. The performance of phenolic nylon is attributable to its forming high temperature chars.

The trends indicate that "THERMO-LAG" T-500 is considerably more efficient than phenolic nylon in "low heat flux, high enthalpy environments".

CONCLUSIONS.

"THERMO-LAG" T-500 is more effective than phenolic nylon when used as a thermal protection system in a low heat flux, high enthalpy environment, such as will occur on the aft body of a low $\frac{W}{C_D A}$ vehicle entering at shallow angles. The "THERMO-LAG" T-500, when sprayed over a substrate, maintains the temprature of the substrate below the sublimation temperature of 530°F. The phenolic nylon maintains the temperature of the substrate below 900°F in all cases.

In the stagnation region at 30 BTU ft^2sec, enthalpy 3500 BTU lb, the "THERMO-LAG" T-500 formed a stable nonconsumable debris matrix. The phenolic nylon receded rapidly at these conditions.

The "THERMO-LAG" T-500 sprayed coating adhered well to the substrate throughout all tests.

APPENDIX A
PERFORMANCE MECHANISM

To facilitate interpretation of the data derived from this testing program, a brief description of the sublimation processes characteristic of each material is presented in conjunction with an energy balance for a typical heat shield material.

During the steady-state ablation and sublimation of "THERMO-LAG" T-500, the material exists in one of the three states indicated below:

1. Virgin material as applied.
2. Pyrolyzed carbonaceous char.
3. A transition state in which the properties of the material range from State 1 to State 2.

As the virgin material attains calorobic temperature, the inorganic subliming salt undergoes a phase change from solid to vapor. The endothermic nature of this phase change provides the thermostatic, temperature-limiting function of the "THERMO-LAG" material. Within the transition state region, a minor volume of gas released by pyrolysis of the binder system adds to the volume of sublimed inorganic vapor. The total vapor volume, transpiring through the pyrolyzed carbonaceous char matrix, provides a major heat absorbing function due to relatively low-temperature endothermic decomposition. Detailed mass transport and kinetic data applicable to this process are available in Emerson Report No. 1139.

The phenolic nylon material, during steady-state ablation, similarly exists in three states; however, the total volume of gas emitted is due to pyrolysis of hydrocarbon polymers, a process providing no temperature limitation. Within the carbonaceous char matrix, the hydrocarbon gases undergo thermocatalytic cracking, an endothermic process occurring at a temperature significantly higher than that at which the sublimed inorganic vapors of the "THERMO-LAG" material endothermically decompose. Upon release to the atmosphere, the catalytically cracked phenolic nylon gases are subject to exothermic reaction with oxygen.

Referring to the following diagram, an energy balance can be made on an element of material in the process of steady-state ablation.

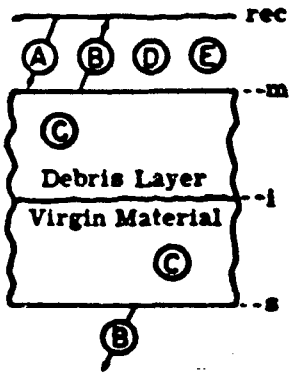

Where A represents incoming energy, B represents outgoing energy, C represents internal energy absorbed, D represents external energy absorbed, and E represents external energy released, the energy balance equation would take the form:

$$A + E = B + C + D$$

Under conditions of steady-state ablation, incoming energy terms are:

convection $h(T_{rec} - T_m)$

radiation $\sigma \epsilon T_{rec}^4$ from equilibrium or non-equilibrium shock front.

Outgoing energy terms are:

re-radiation $\sigma \epsilon T_m^4$

conduction $\frac{k_a \rho_a}{\dot{m}_a}(T_i - T_s)$ into substrate heat sink.

Considering the conservation of matter equation $\dot{m}_a = \dot{m}_v + \dot{m}_d$ where $\dot{m}_a$ is the overall mass loss rate of the ablative material, $\dot{m}_v$ is the mass rate of liquid or vapor formed, and $\dot{m}_d$ is the mass rate of debris or char formed, $\dot{m}_v$ and $\dot{m}_d$ can be represented by,

$$\dot{m}_v = \dot{m}_a\left(\frac{\rho_a - \rho_d}{\rho_a}\right)$$

$$\dot{m}_d = \dot{m}_a\left(\frac{\rho_d}{\rho_a}\right)$$

Typical terms for internal energy absorption are:

Heat of vaporization $\dot{m}_a \left(\frac{\rho_a - \rho_d}{\rho_a}\right) Q_v$

Heat of fusion $\dot{m}_a \left(\frac{\rho_a - \rho_d}{\rho_a}\right) Q_f$

Heat of sublimation $\dot{m}_a \left(\frac{\rho_a - \rho_d}{\rho_a}\right) Q_s$

Sensible heating of gases in the char matrix $\dot{m}_a \left(\frac{\rho_a - \beta}{\rho_a}\right)(T_m - T_i) c_{gv}$

Sensible heating of char material $\dot{m}_a \left(1 - \frac{\rho_a - \rho_d}{\rho_a}\right)(T_m - T_i) c_d$

Sensible heating of virgin material $\dot{m}_a (T_i - T_0) c_a$

Dissociation within char matrix $\dot{m}_a \left(\frac{\rho_a - \rho_d}{\rho_a}\right)(T_m - T_i) B$

Typical terms for external energy absorption are:

Transpiration of gases in boundary layer

Char material $\alpha_{gd} \dot{m}_a \left(\frac{\rho_a}{\rho_a}\right)(T_{rec} - T_m) c_{gd}$

Virgin material $\alpha_{gv} \dot{m}_a \left(\frac{\rho_a - \rho_d}{\rho_a}\right)(T_{rec} - T_m) c_{gv}$

Dissociation in boundary layer $\beta_{gv} \dot{m}_a \left(\frac{\rho_a - \rho_d}{\rho_a}\right)(T_{rec} - T_m) B$

Typical terms for external energy release are:

Combustion of char material, combustion parameter, $\frac{O_2 H_d}{(h_{rec} - h_m)} \left(\frac{\rho_d}{\rho_a}\right)$

Combustion of gases, combustion parameter, $\frac{O_2 H_v}{(h_{rec} - h_m)} \left(\frac{\rho_a - \rho_d}{\rho_a}\right)$

The over-all heat balance of a heat shield material may then be expressed as follows:

$$F \sigma \epsilon (T_{rec}^4 - T_m^4) + \{[T_{rec} - T_m][h - \dot{m}_a (\xi \alpha_{gv} c_{gv} + \xi \beta_{gv} B + (1-\xi)(\alpha_{gd} c_{gd}))]\}$$

$$\left\{1 + \frac{O_2 (\xi H_v + (1-\xi) H_d}{(h_{rec} - h_m)}\right\} - \xi \dot{m}_a [(T_m - T_i)(c_{gv} + B) + Q_v + Q_f + Q_s]$$

$$- \dot{m}_a [c_a (T_i - T_s) + c_d (1 - \xi)(T_m - T_i)] = \frac{k_a \rho}{\dot{m}_a} (T_i - T_s)$$

In the case of phenolic nylon, the heat of sublimation, Q_s is not applicable. In the case of the "THERMO-LAG" material, neither heat of fusion, Q_f, heat of vaporization Q_v, nor the combustion parameters are applicable.

APPENDIX B
PLASMADYNE HYPERTHERMAL TUNNEL

The apparatus in which the tests discussed in this report were conducted consisted of the following components:

1. ARC PLASMA GENERATOR.

A schematic diagram of this unit is contained in Figure 2. The unit consists of a water-cooled enclosure containing a conical, tungsten-tipped rear cathode discharging to a forward copper annulus anode. The electrode gas, nitrogen, is tangentially introduced into the arc chamber, thus providing gas vortex arc stabilization as it is heated to a selected high-energy state.

2. MIXING CHAMBER.

The heated gas from the arc plasma generator is discharged into the mixing chamber where oxygen is introduced through a ring injector in the proper proportion to simulate air.

3. AERODYNAMIC NOZZLE.

The simulated air plasma flows from the mixing chamber to a water-cooled, contoured, supersonic aerodynamic nozzle. This nozzle has a 3-inch exit diameter through which the gas is expanded to a velocity of mach 3.

4. TEST SECTION.

The test section consists of a double-walled, water-cooled cylindrical chamber 30 inches in diameter and 8 feet in length. Side views of the models as the test in progress were provided by two opposing pyrex viewing ports. Two 1-1 2-inch quartz viewing ports located in the downstream end of the test section enabled optical pyrometer readings to be made during the test. A pneumatically operated, water-cooled model insertion system additionally provides a conduit for instrumentation leads. Figure 4 shows a test model installed in the insertion system.

5. GAS SYSTEMS.

Gas systems are provided for pressure reduction, metering, and delivery of oxygen and nitrogen to the appropriate chambers.

6. VACUUM SYSTEM.

The arrangement of the vacuum system is shown in Figure 1. The system consists of a tube-type heat exchanger located at the test section exit, a Roots-type blower, and mechanical vacuum pumps.

7. POWER SUPPLY SYSTEM.

Eight rectifiers, each rated at 40-kilowatt continuous duty and 60-kilowatt peak, provide the D.C. power to the test system at an open circuit voltage of 80.

8. SYSTEM INSTRUMENTATION.

a. Calorimeter. A 5/8-inch diameter, water-cooled copper calorimeter was used to measure the stagnation point cold-wall heat transfer properties of the supersonic plasma stream. The temperature rise of a controlled and metered cooling water flow was monitored.

b. Pitot Probe. The pitot pressure of the plasma stream was measured by means of a probe device equipped with sensitive, rapid-response, direct-reading instruments.

c. Miscellaneous System Instrumentation. Suitable instruments were provided for measurement of gas flow rates, pressures, and temperatures; power to electrodes; and cooling water temperatures, and flow rates. A Bolex color movie camera was used to make a pictorial record of the model profile during test.

d. Total Enthalpy Probe. Total enthalpy of the plasma stream was measured by an energy balance on the entire system. The accuracy of the energy balance was assured by previous comparison with total enthalpy measurements from a total enthalpy probe. This probe extracted and cooled a known amount of gas from the plasma stream. Total enthalpy was then calculated from the cooling load imposed upon the probe.

9. MODEL INSTRUMENTATION.

a. Optical Pyrometer. A Leeds and Northrop portable, battery-operated optical pyrometer was used to measure the stagnation region surface temperature of models during test.

b. Recording Oscillograph. A 14-channel Midwestern Instrument Co., Model 621 F direct-printing oscillograph, was used to provide temperature traces of all model and calorimeter thermocouples.

APPENDIX C
ANALYSIS OF SHAPE OF SIDEWALL THERMOCOUPLE CURVES

An analysis of the side wall thermocouple curves revealed that their shape was similar to that predicted by the equation

$$\left[\frac{T_s - T_i}{T_g - T_i}\right] = \left[1 - e^{-\frac{\uparrow k_s \rho_s}{W_s C_s W_s}}\right]$$

This equation, plotted in Figure 54, predicts temperature histories underneath coatings which do not recede with time and which are subjected to a constant, sudden temperature rise of their exposed surface. (Ref. 9.)

An equation which predicts temperature histories under coatings which do recede with time, with constant surface temperatures, (Ref. 1), is

$$\left[\frac{T_s - T_i}{T_g - T_i}\right] = \left[e^{\frac{(x^{n+1} - x_n)\rho_s C_s}{k_s}}\right]$$

This equation is also plotted in Figure 54, and is labeled "moving boundary equation".

In order to study the shape of these curves alone, the time scale was nondimensionalized with respect to Θ, the time for the substrate to reach 99 percent of the driving temperature.

Post-test model inspection indicated that coating thicknesses were essentially the same as originally applied to the models. Therefore, the shape of the thermocouple curves would be expected to follow the predictions of the nonreceding equation rather than the moving boundary equation predictions.

ILLUSTRATIONS

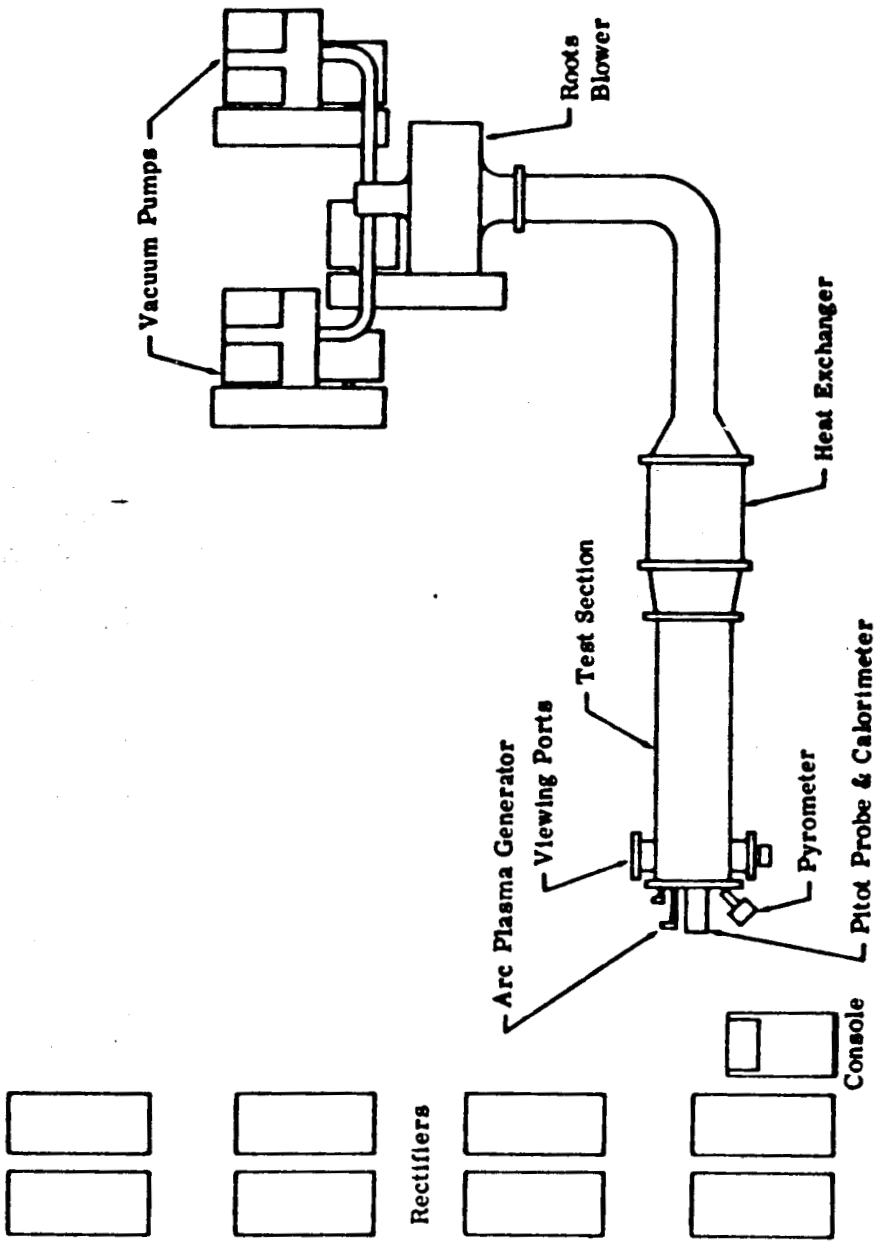

Figure 1. Schematic of Hyperthermal Test Facility

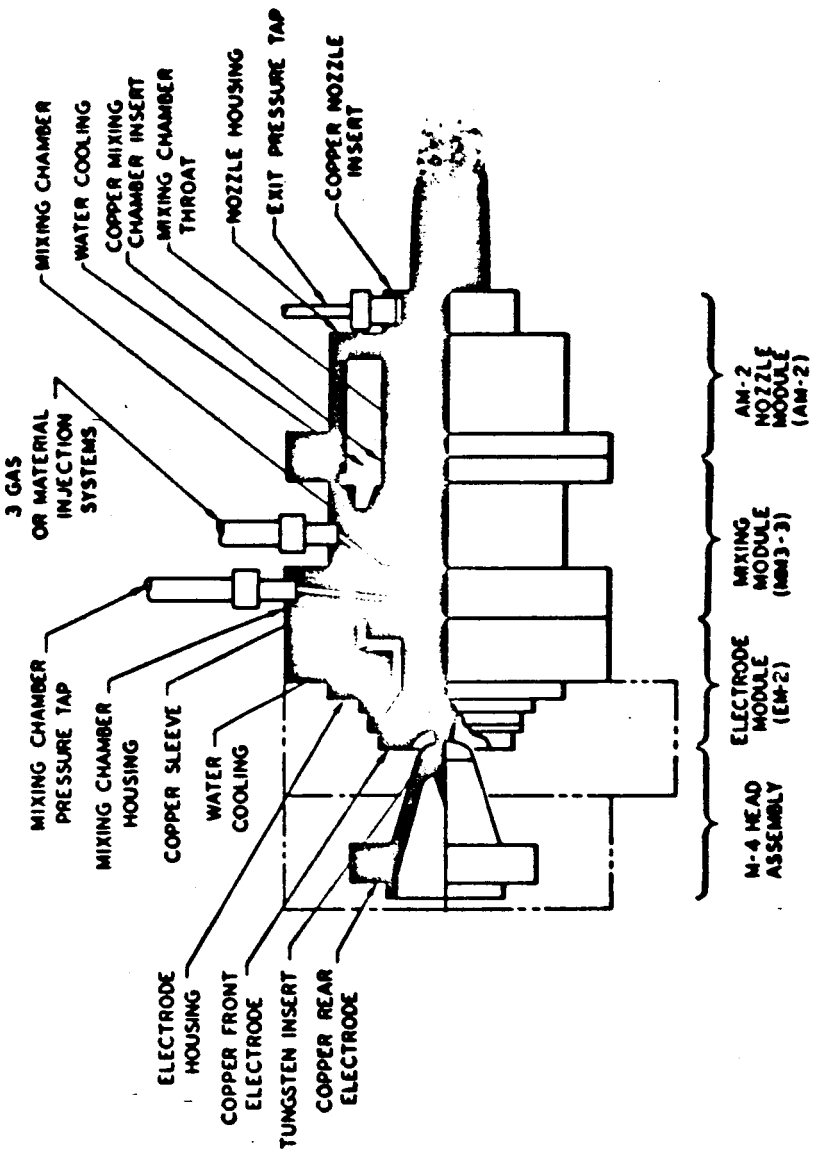

Figure 2. Schematic of Arc Plasma Generator

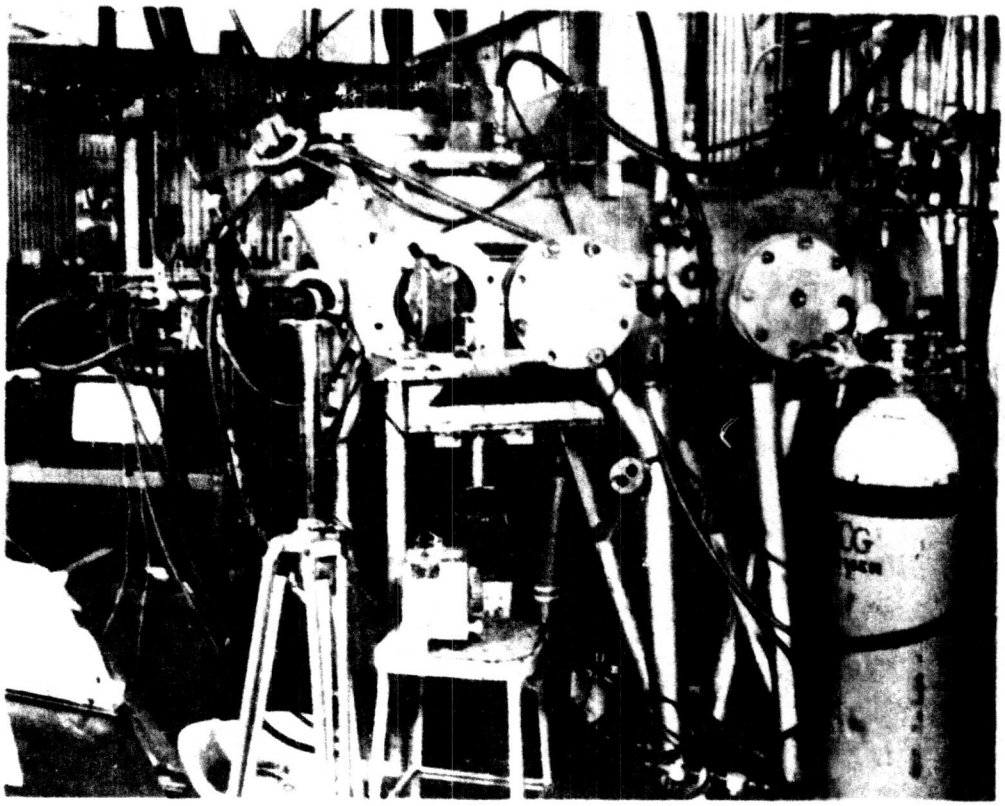

Figure 3. Plasmadyne Hyperthermal Test System

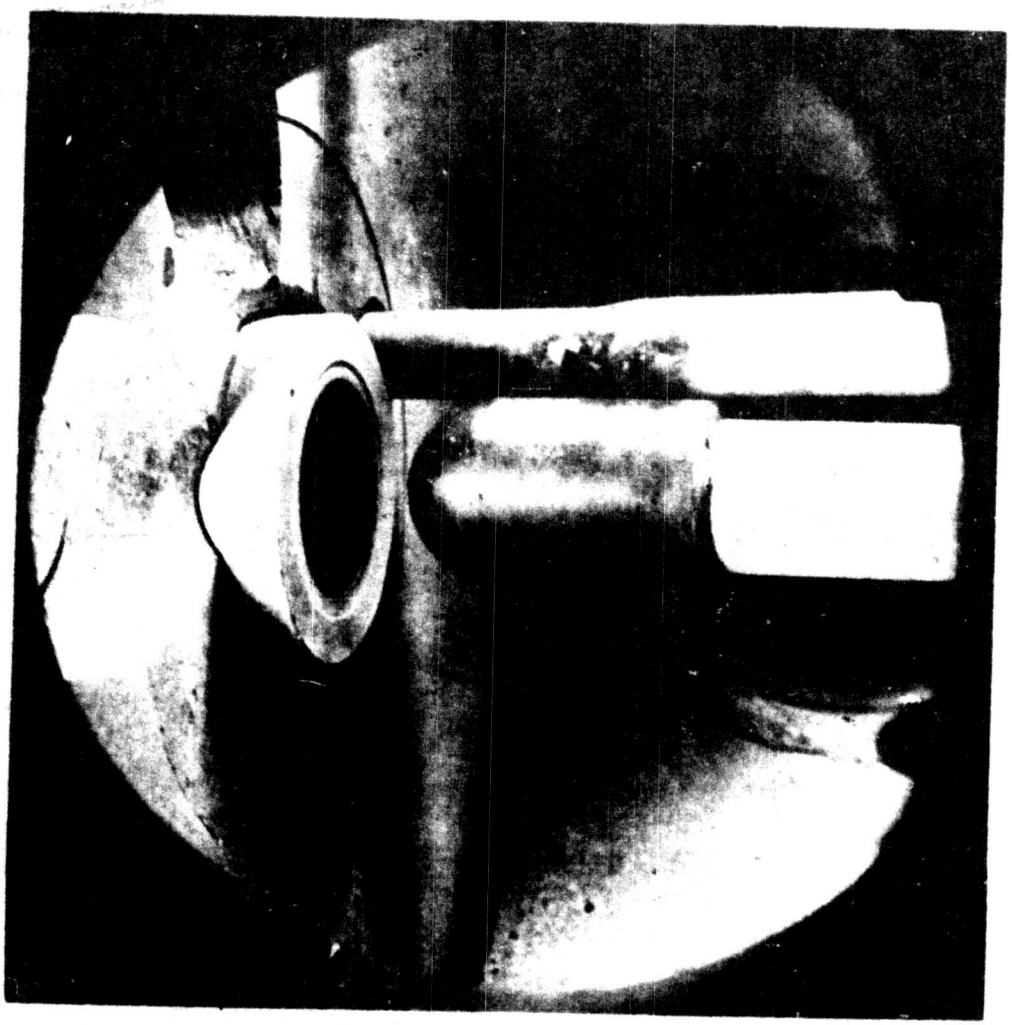

Figure 4. Sting Mounted Model in Front of Plasma Jet Nozzle

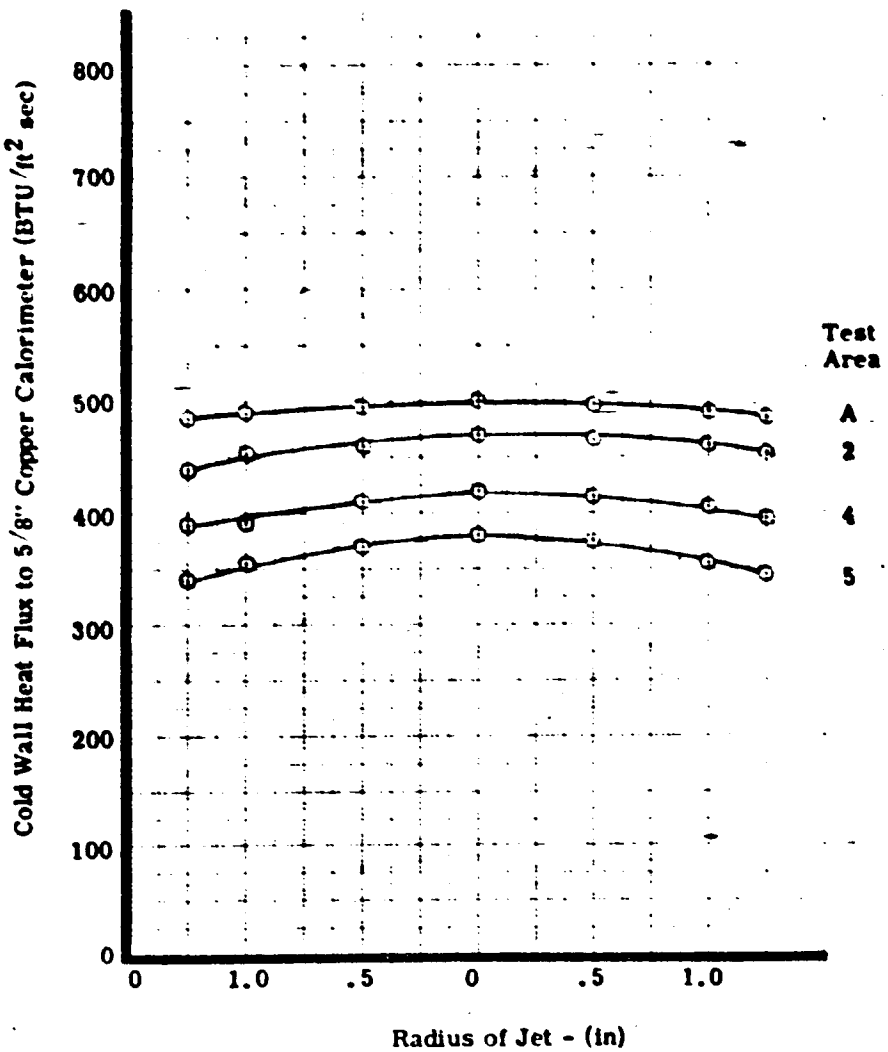

Figure 5. Radial Heat Flux Distribution Across Jet

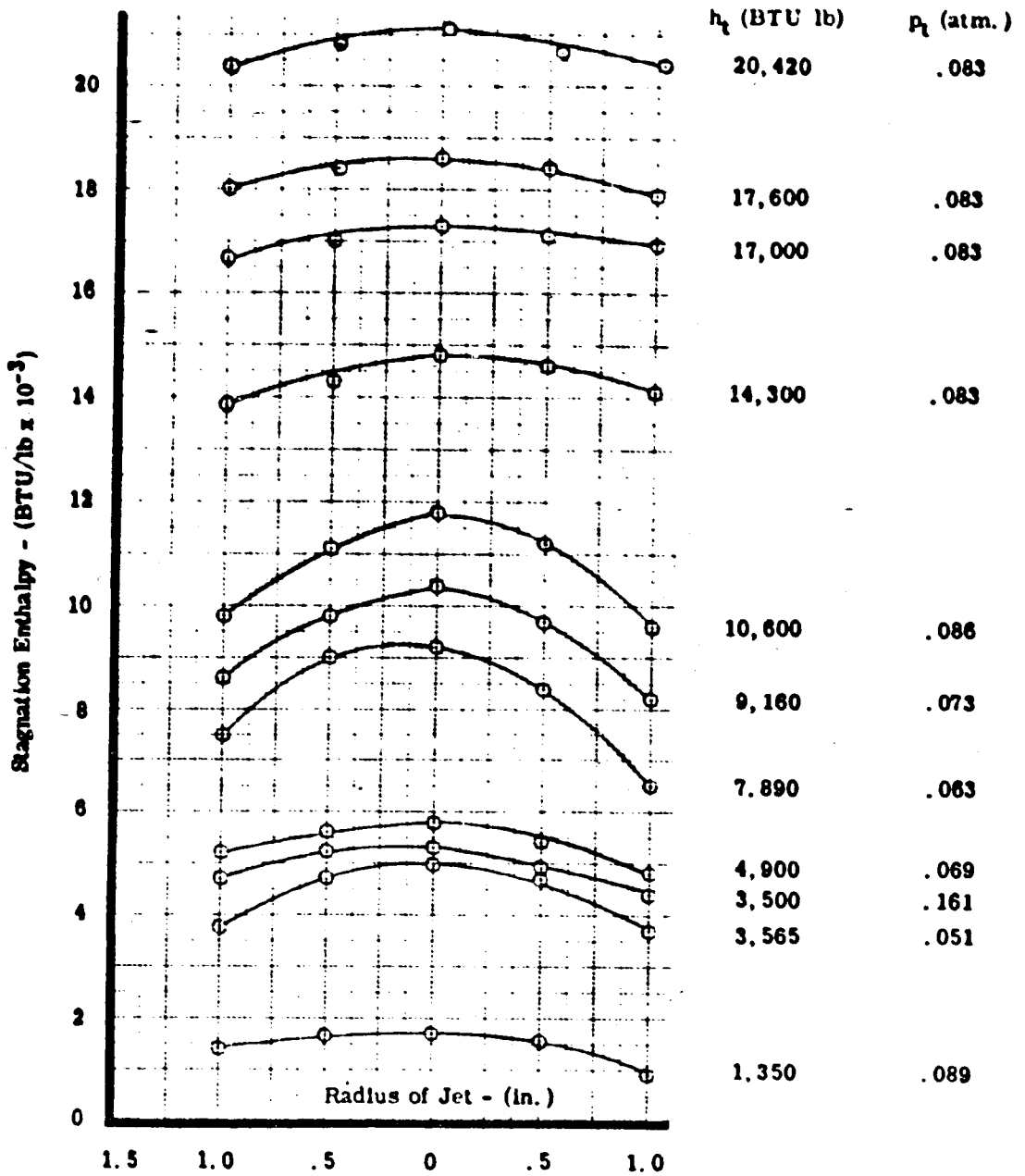

Figure 6. Radial Total Enthalpy Distribution Across Jet

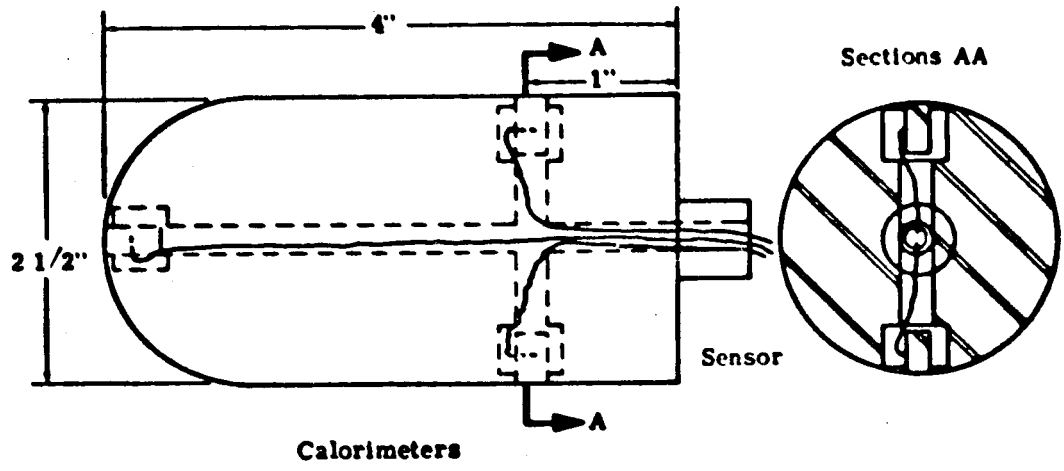

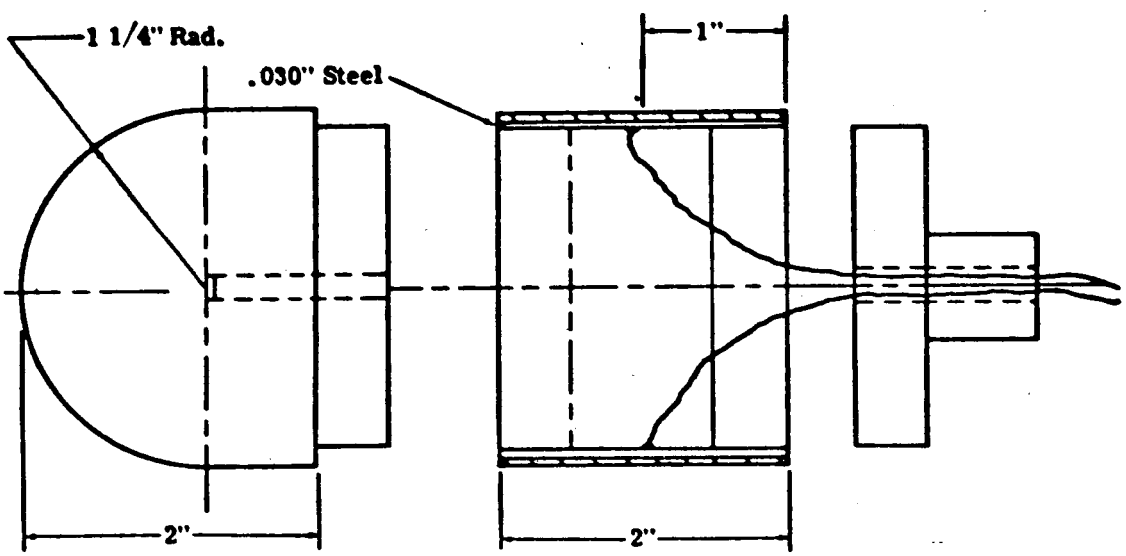

Figure 7. Schematic of Calorimeters and Models

Figure 8. Assembled Model

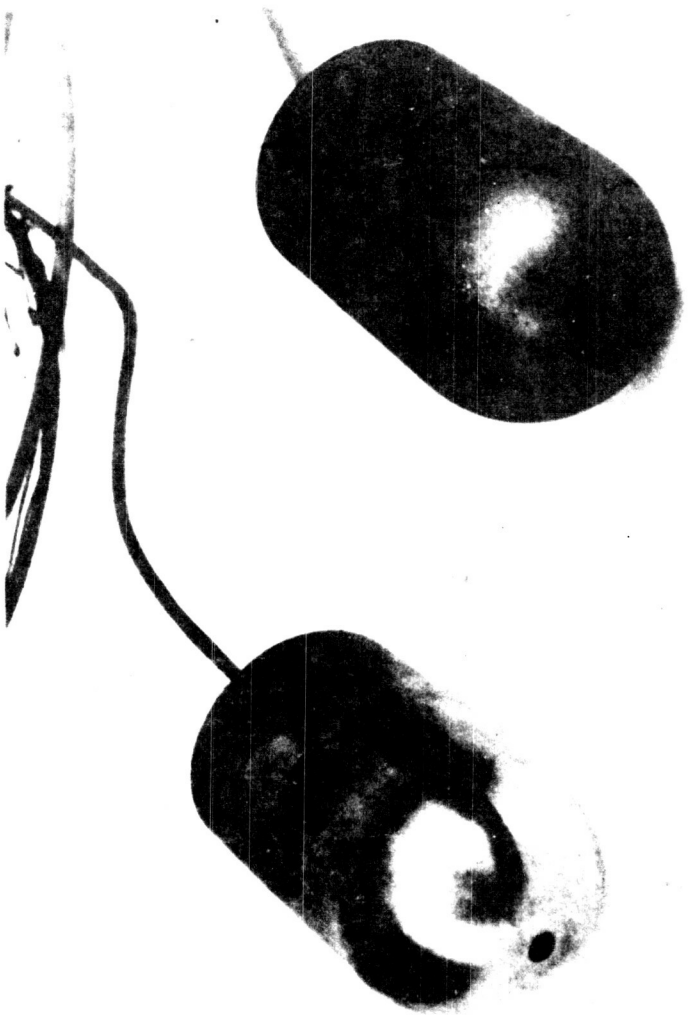

Figure 9. Transient Calorimeters

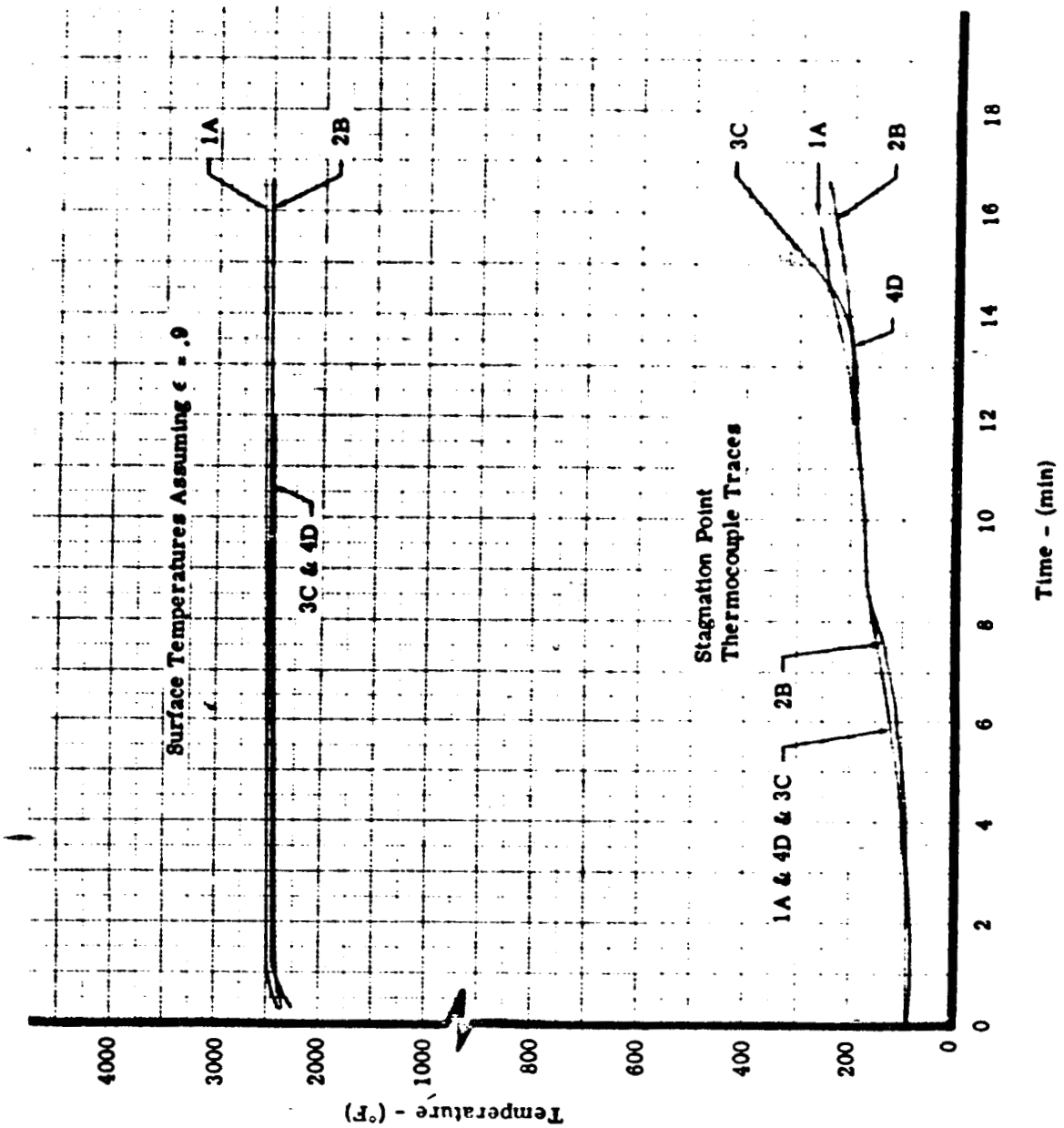

Figure 10. "THERMO-LAG" T-500 Model Data, Test Condition 1

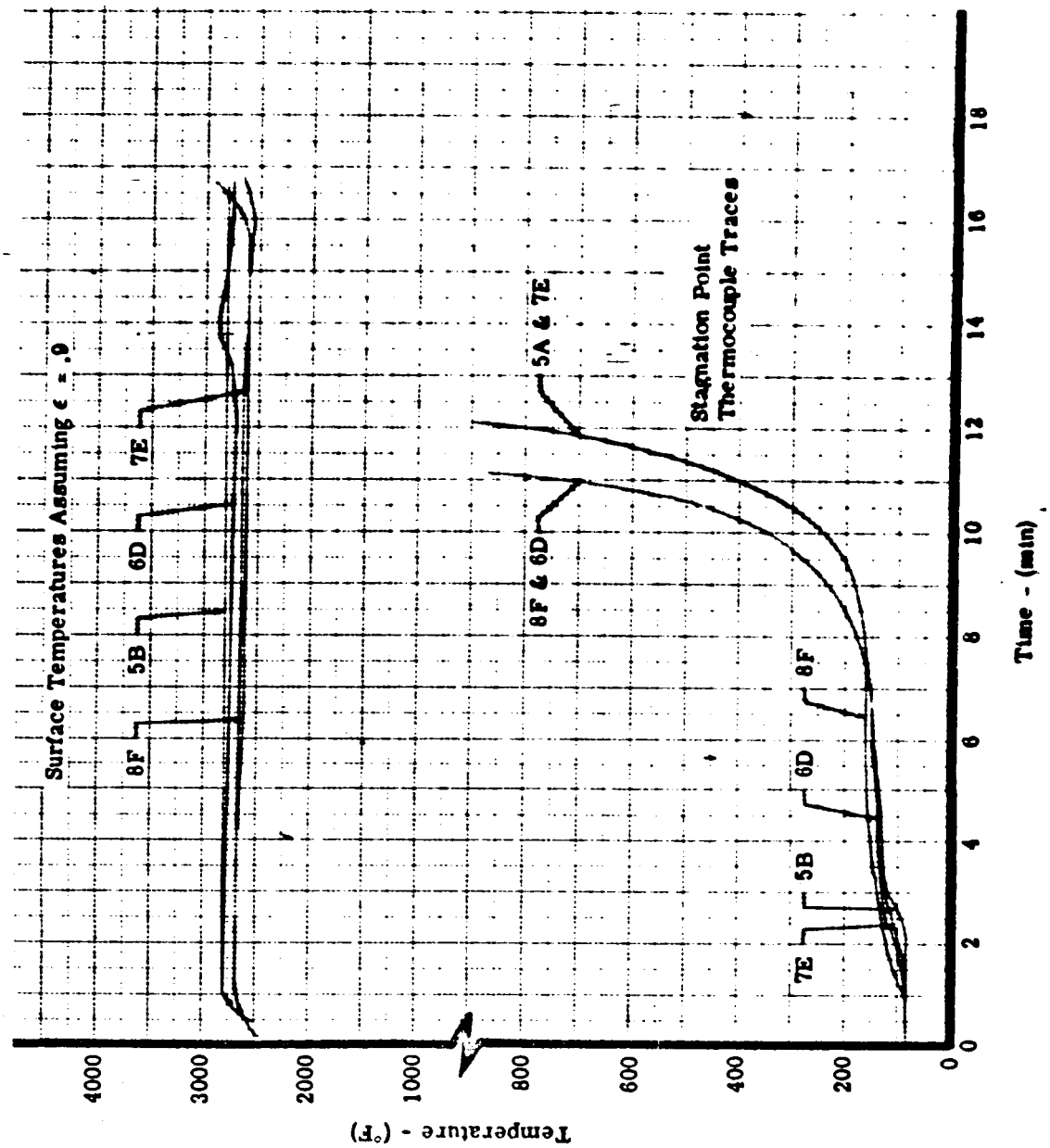

Figure 11. Phenolic Nylon Model Data, Test Condition 1

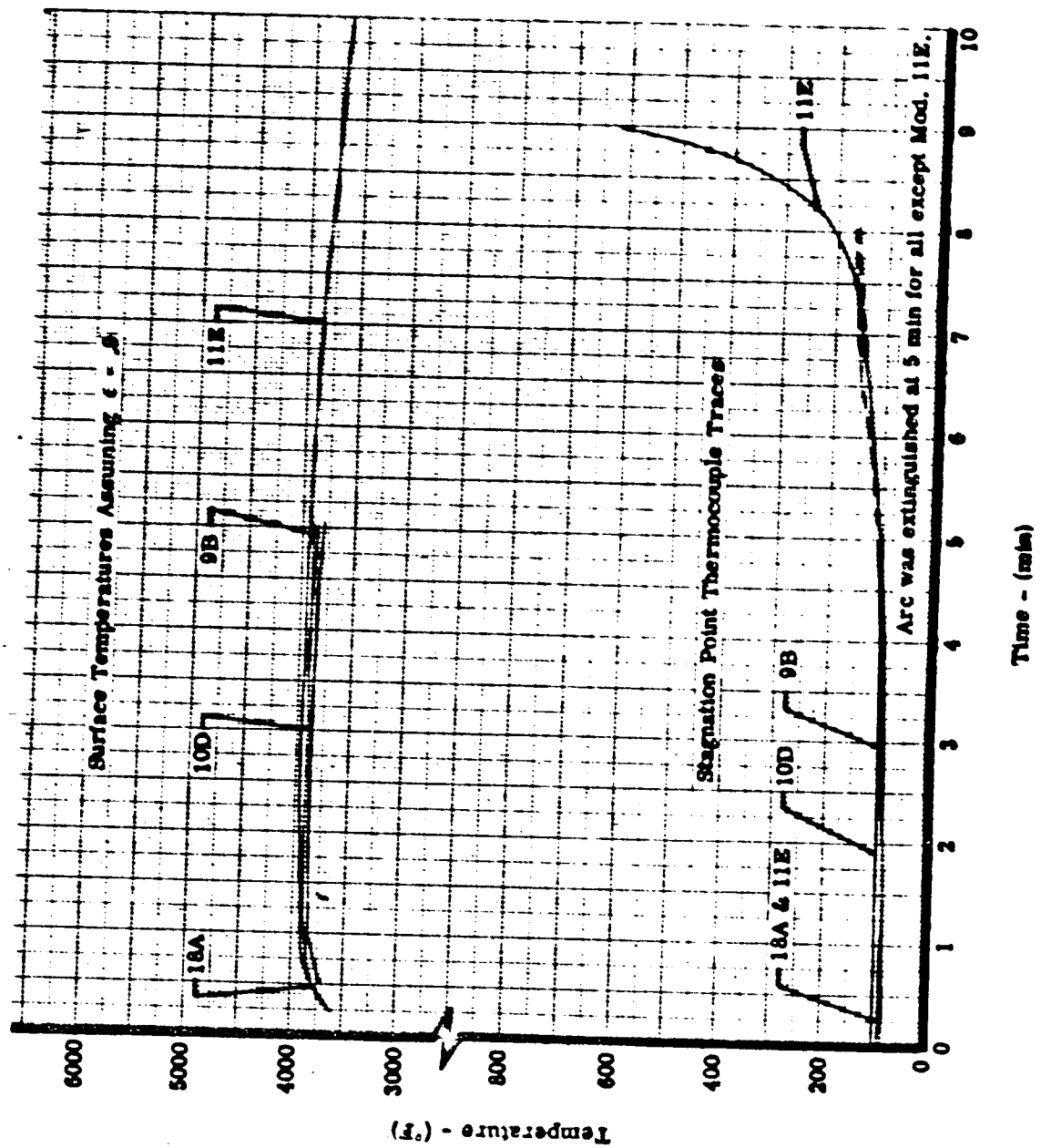

Figure 12. "THERMO-LAG" T-500 Model Data, Test Condition 2

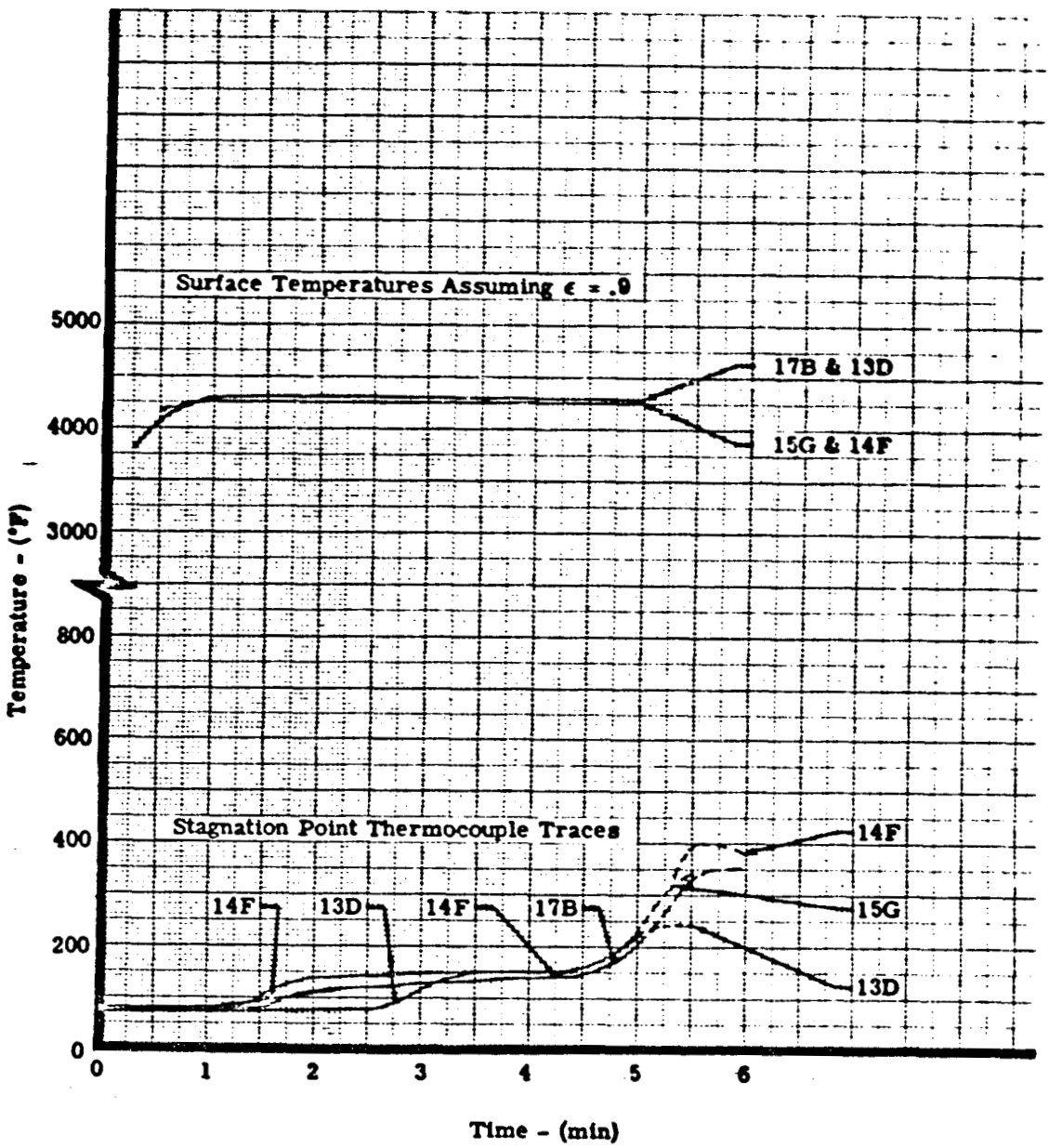

Figure 13. Phenolic Nylon Model Data, Test Condition 2

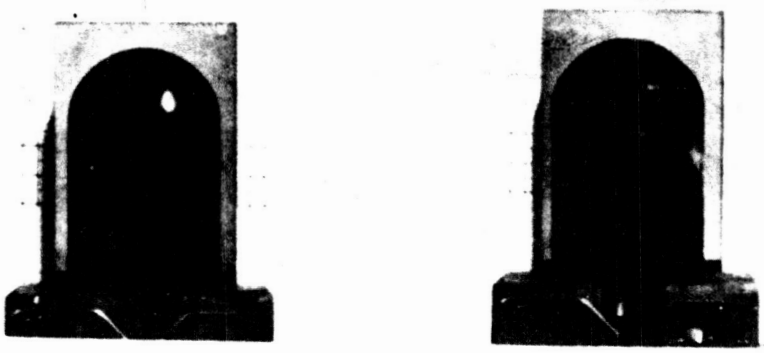

Before

After

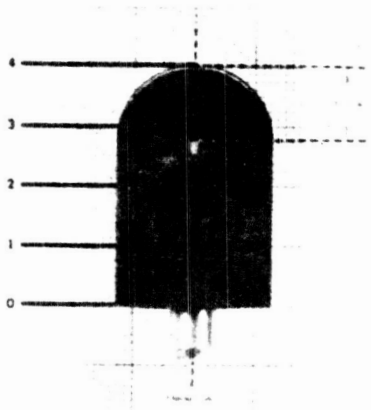

Sectioned View

Figure 14. "THERMO-LAG" T-500 Model 1A, 16.7-Minute Exposure to a Stagnation Enthalpy of 3510 BTU/lb at a Heat Flux of 30.0 BTU/ft^2 sec

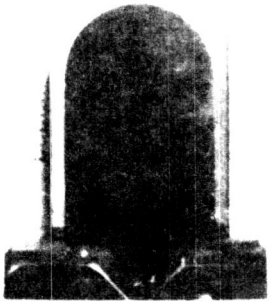

Before

After

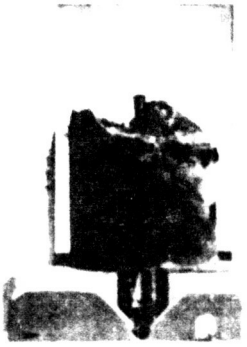

After

Figure 15. Phenolic Nylon Model 5B. 16.7-Minute Exposure to a Stagnation Enthalpy of 3685 BTU/lb at a Heat Flux of 29.5 BTU/ft^2 sec

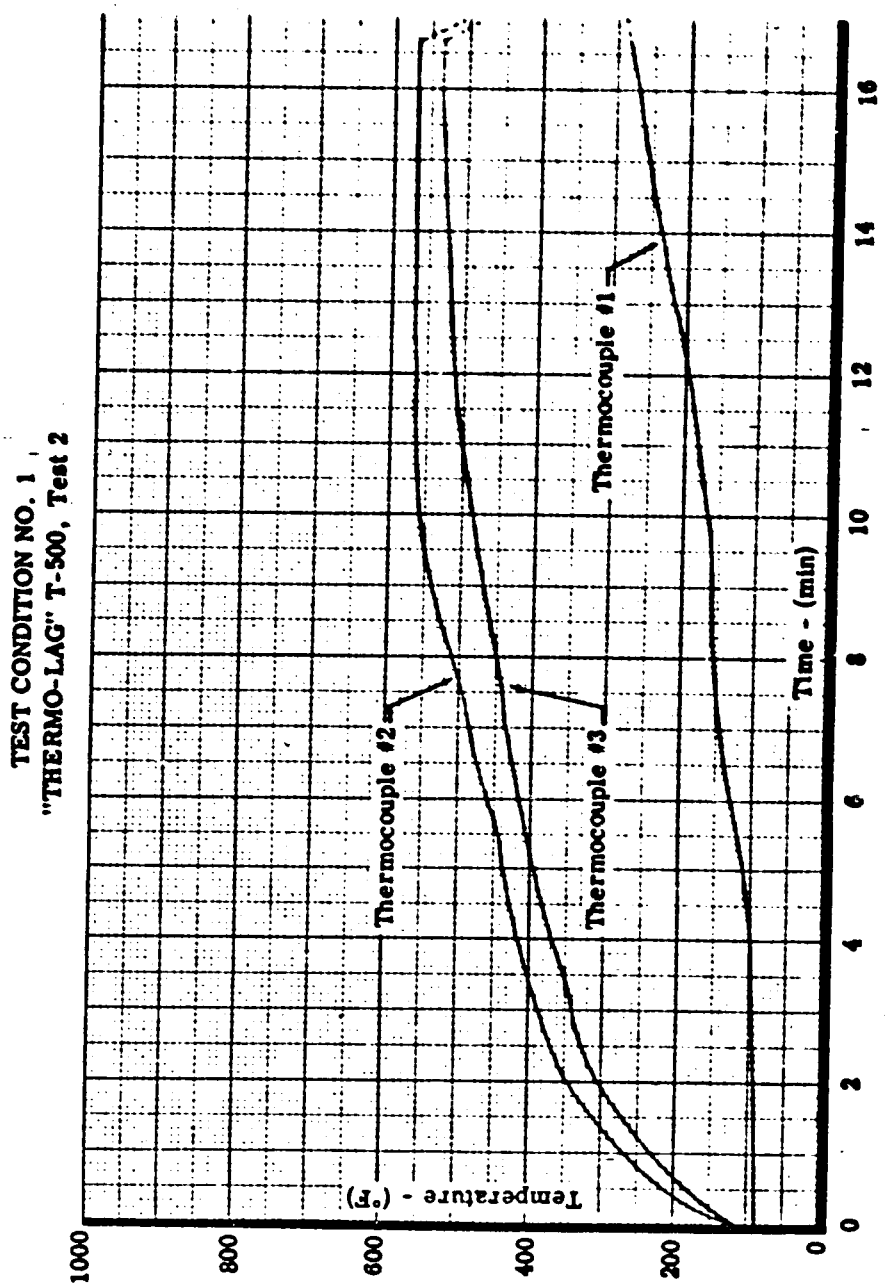

Figure 16. Thermocouple Traces, Model 1A

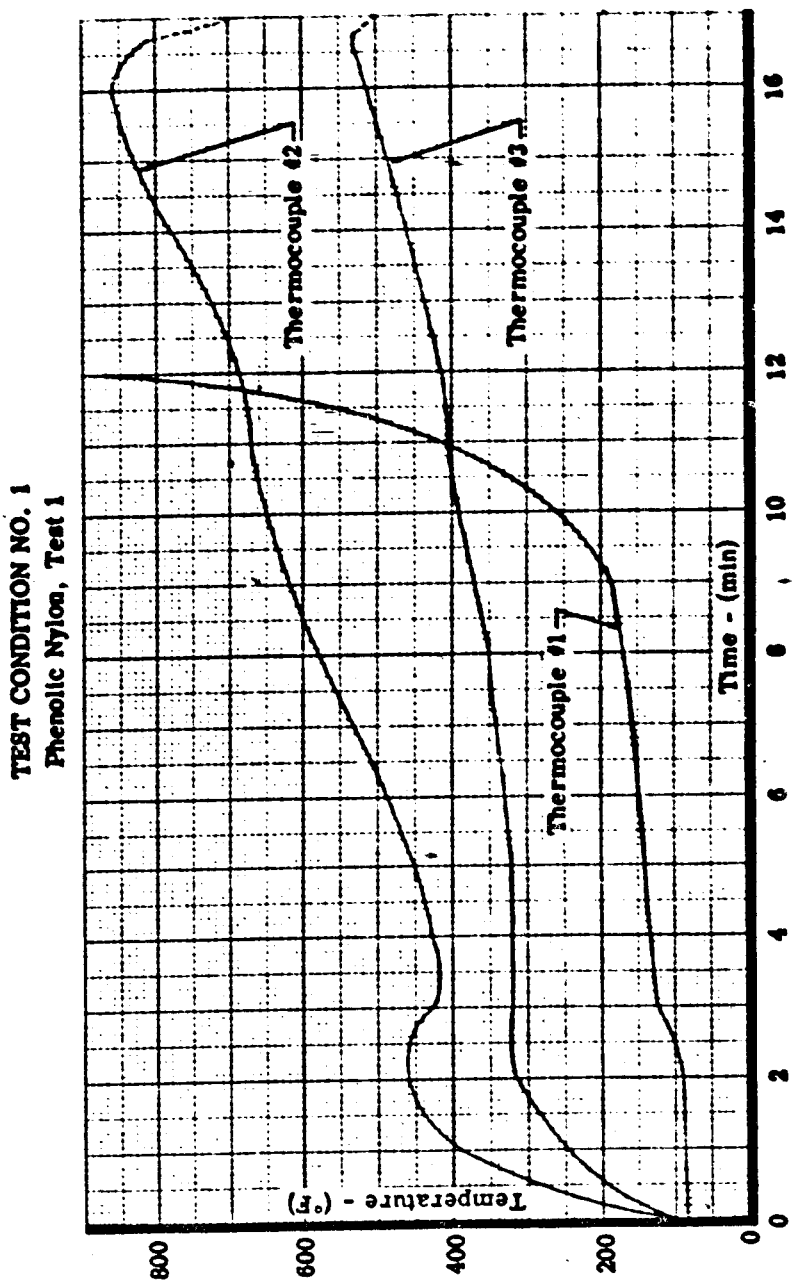

Figure 17. Thermocouple Traces, Model 5B

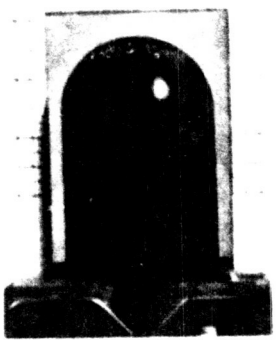

Before

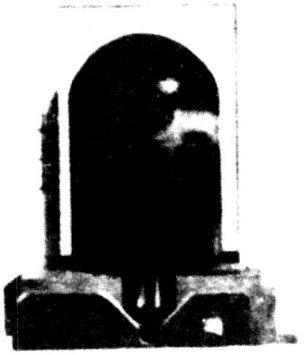

After

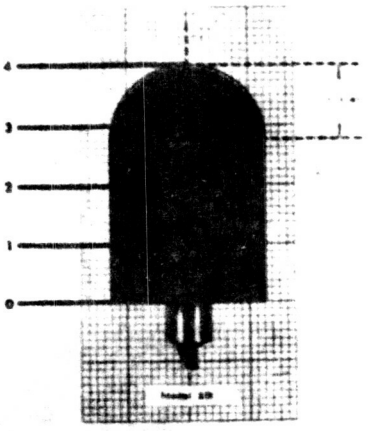

Sectioned View

Figure 18. "THERMO-LAG" T-500 Model 2B, 16.7-Minute Exposure to a Stagnation Enthalpy of 3600 BTU/lb at a Heat Flux of 30.2 BTU/ft^2 sec

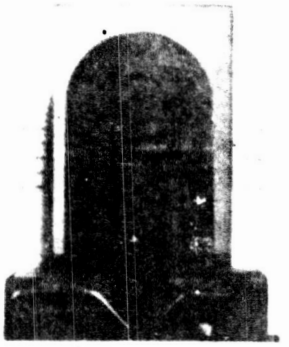

Before

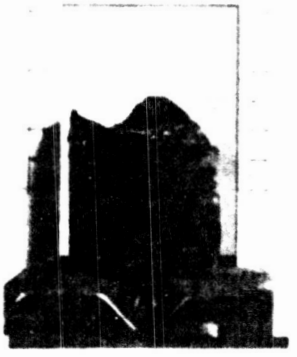

After

Figure 19. Phenolic Nylon Model 6D, 16.7-Minute Exposure to a Stagnation Enthalpy of 3598 BTU lb at a Heat Flux of 29.3 BTU ft^2 sec

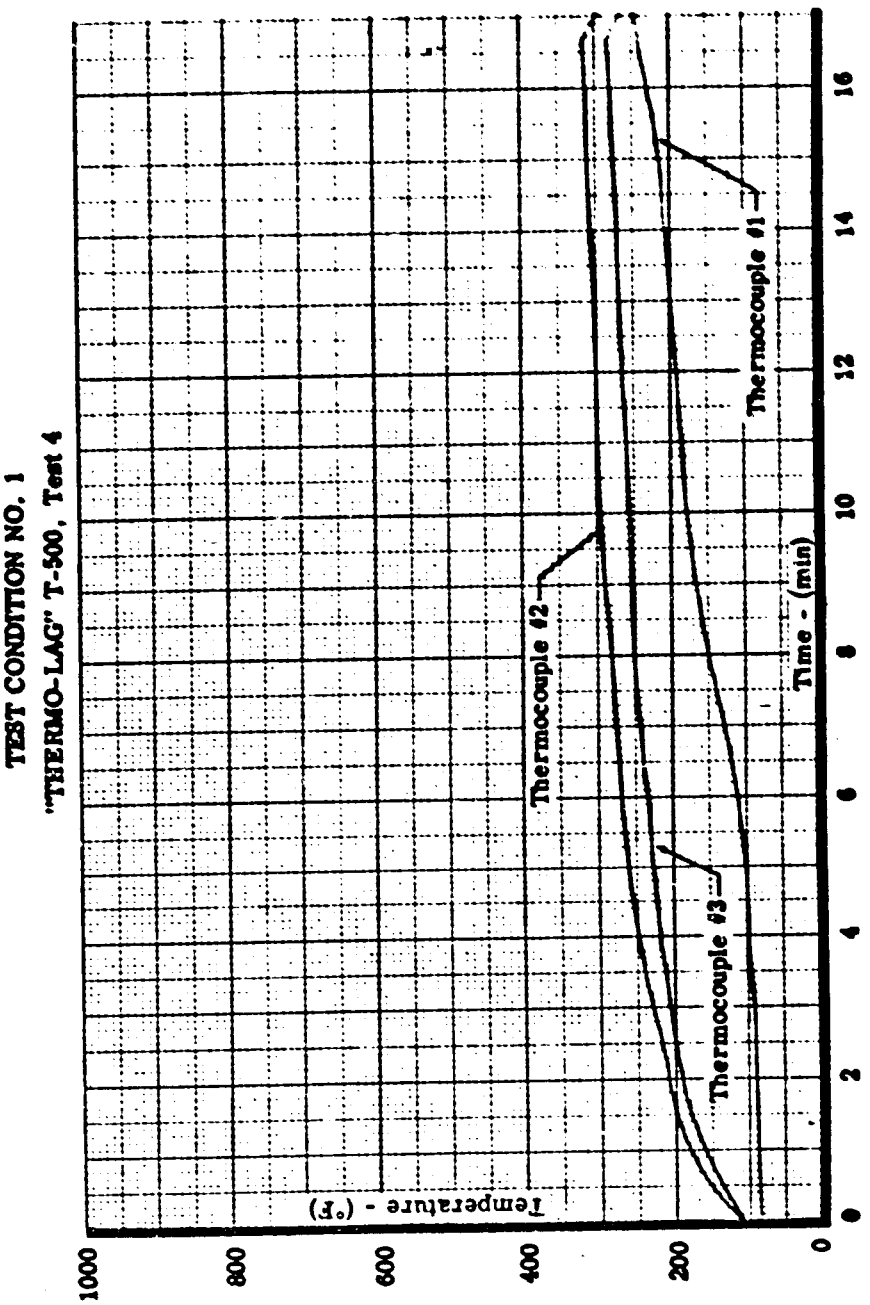

Figure 20. Thermocouple Traces, Model 2B

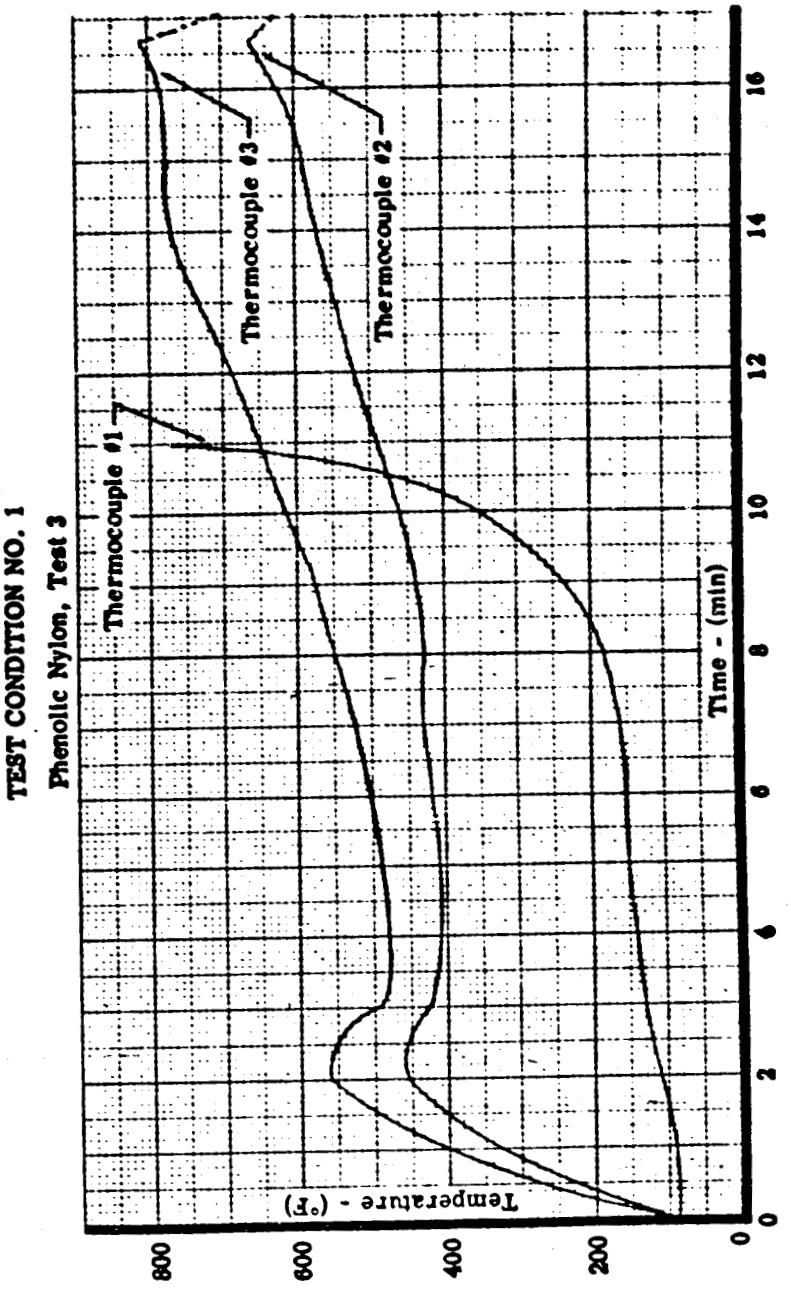

Figure 21. Thermocouple Traces, Model 6D

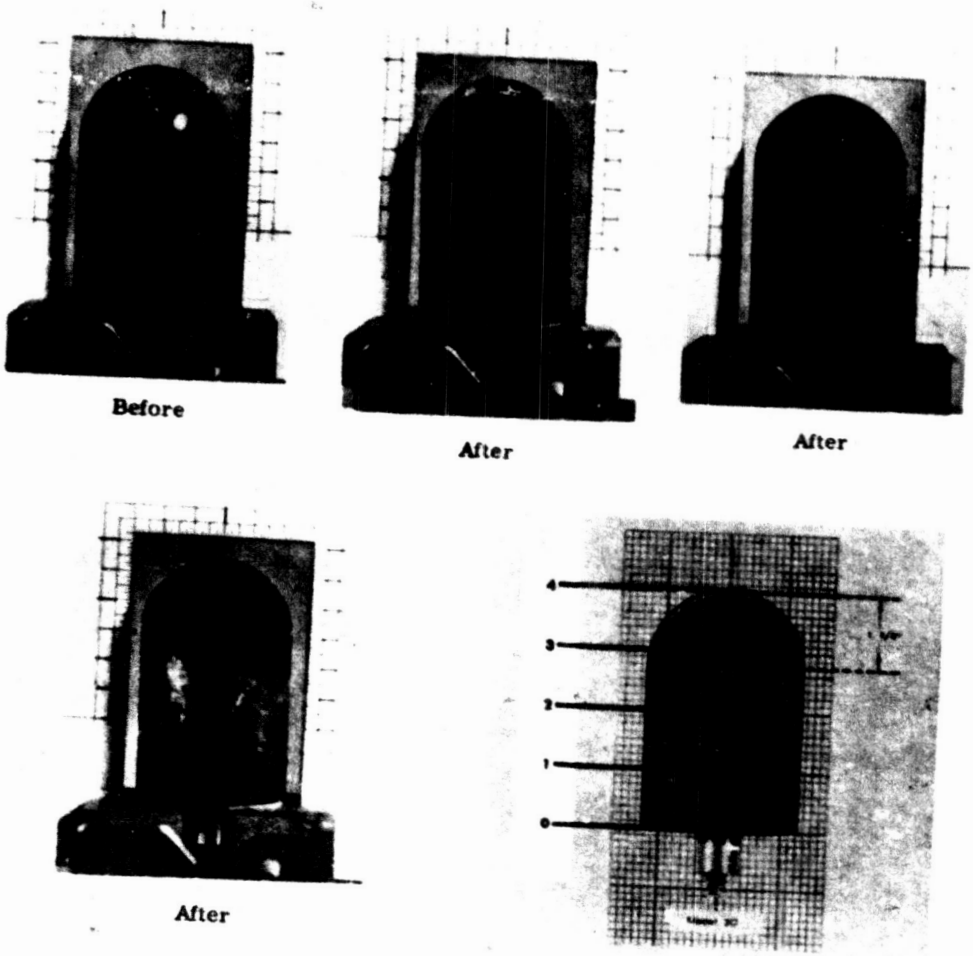

Figure 22. "THERMO-LAG" T-500 Model 3C, 12.7-Minute Exposure to a Stagnation Enthalpy of 3550 BTU/lb at a Heat Flux of 30.3 BTU/ft^2 sec

Before

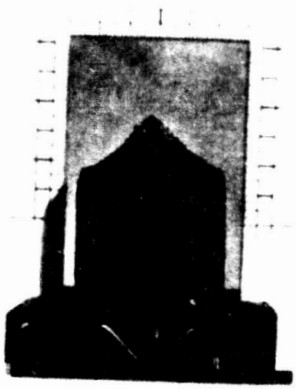

After

After

Figure 23. Phenolic Nylon Model 7E, 16.7-Minute Exposure to a Stagnation Enthalpy of 3580 BTU/lb at a Heat Flux of 29.4 BTU/ft^2 sec

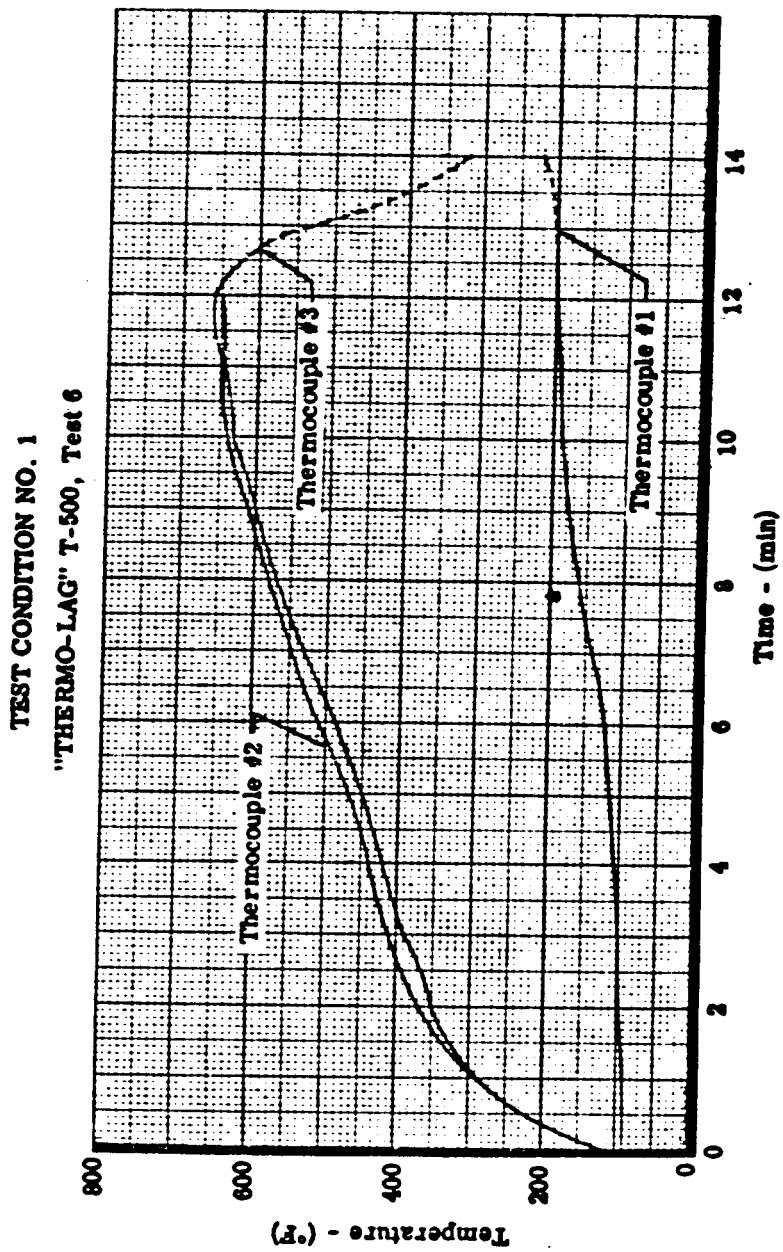

Figure 24. Thermocouple Traces, Model 3C

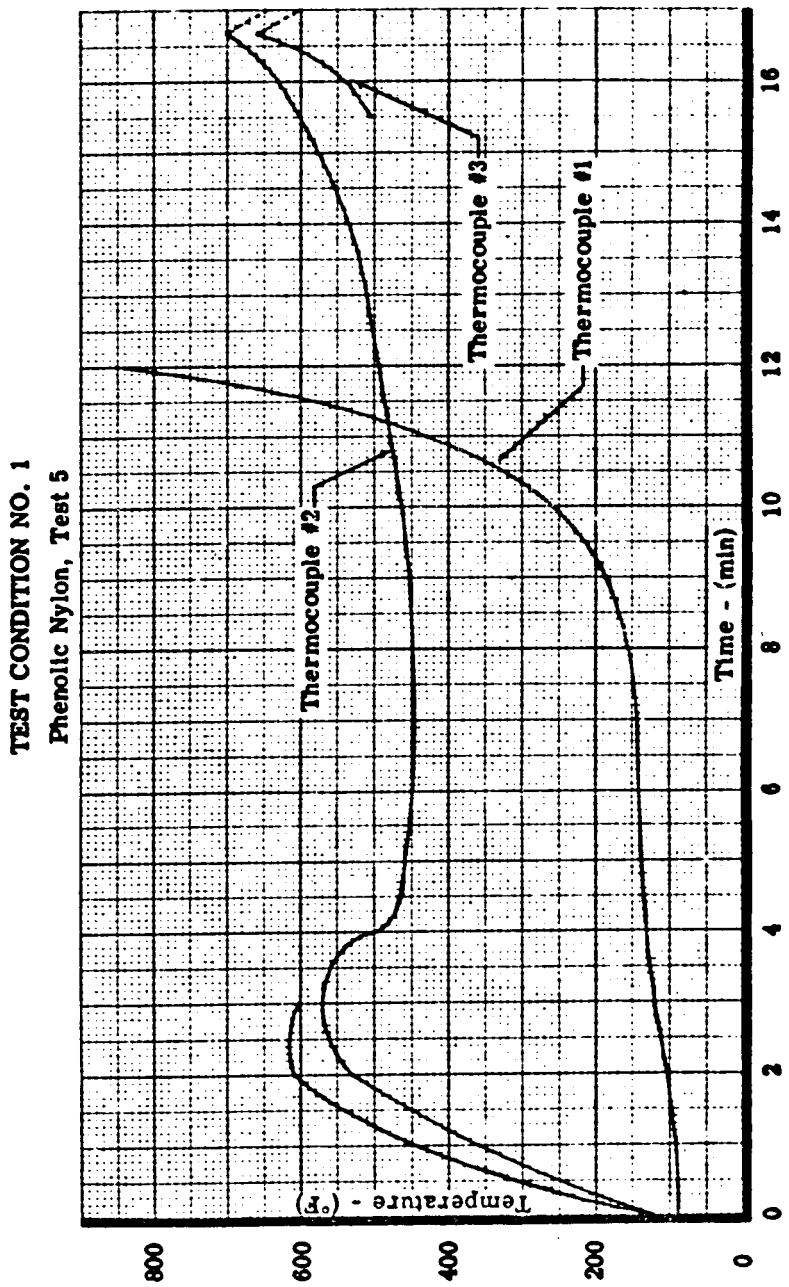

Figure 25. Thermocouple Traces, Model 7E

Before After After

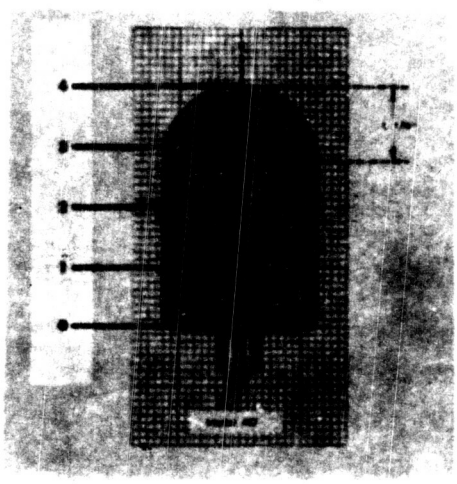

Sectioned View

Figure 26. "THERMO-LAG" T-500 Model 4D, 12.7-Minute Exposure to a Stagnation Enthalpy of 3610 BTU/lb at a Heat Flux of 30.2 BTU/ft^2 sec

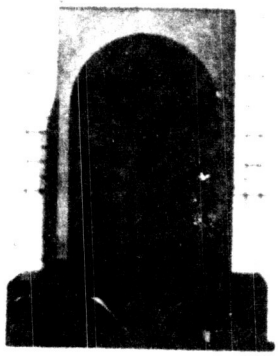

Before

After

Figure 27. Phenolic Nylon Model 8F, 16.7-Minute Exposure to a Stagnation Enthalpy of 3575 BTU/lb at a Heat Flux of 29.6 BTU/ft^2 sec

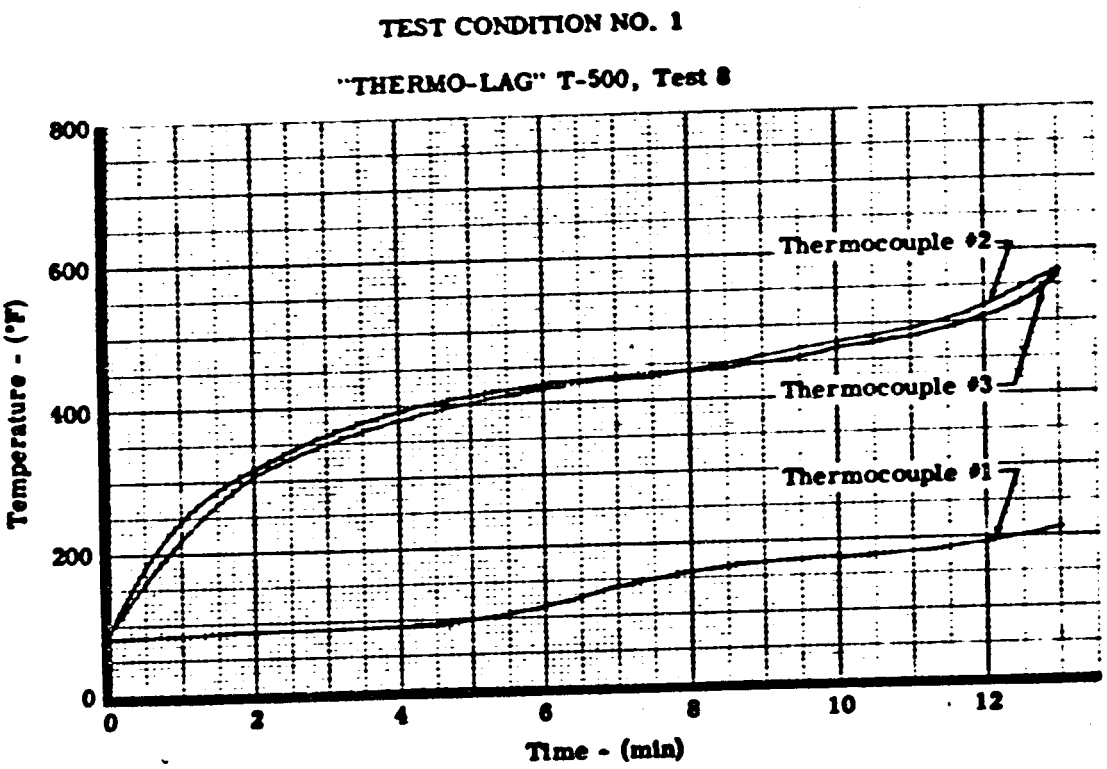

Figure 28. Thermocouple Traces, Model 4D

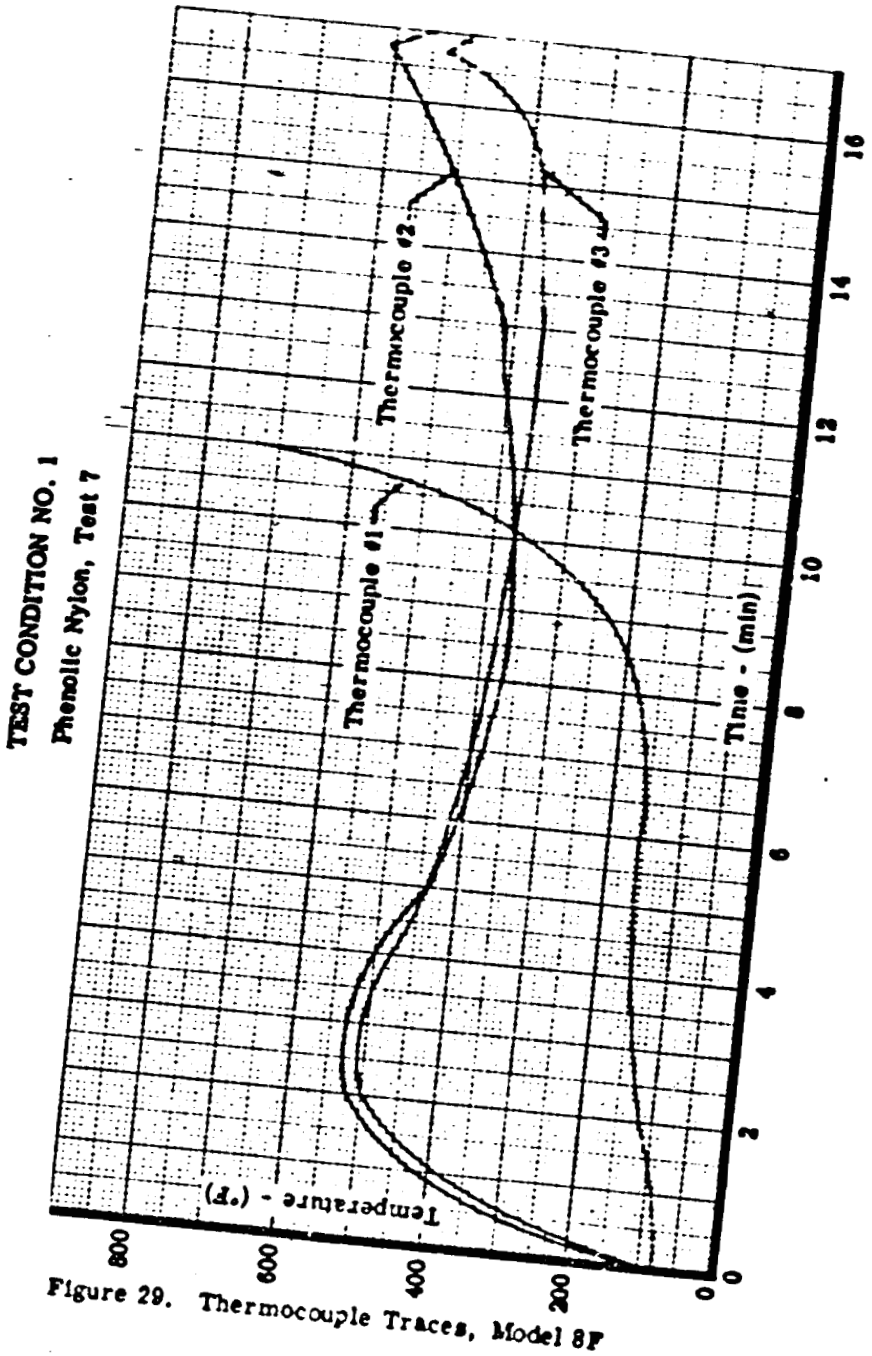

Figure 29. Thermocouple Traces, Model 8F

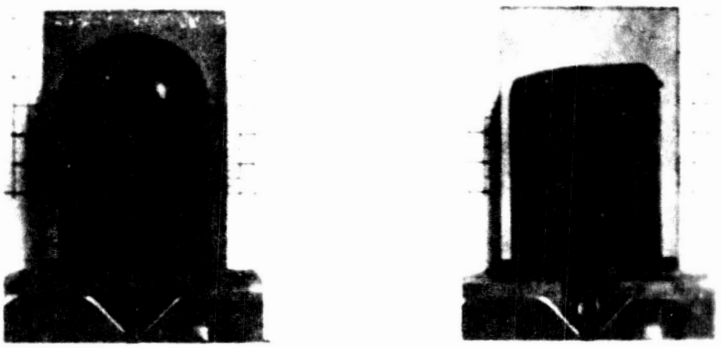

Before

After

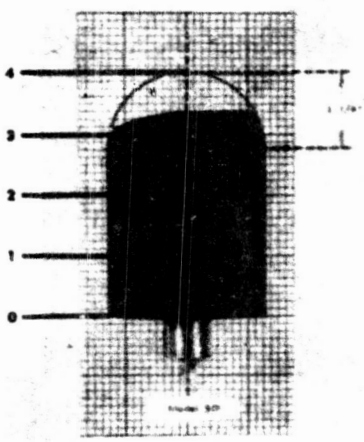

Sectioned View

Figure 30. "THERMO-I.AG" T-500 Model 9B, 5-Minute Exposure to a Stagnation Enthalpy of 17,550 BTU/lb at a Heat Flux of 360.6 BTU/ft^2 sec

Before

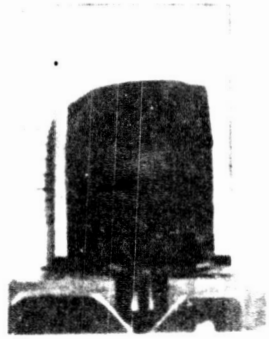

After

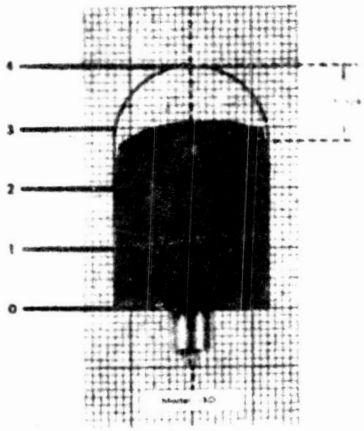

Sectioned View

Figure 31. Phenolic Nylon Model 13D, 5-Minute Exposure to a Stagnation Enthalpy of 17,480 BTU/lb at a Heat Flux of 355.6 BTU/ft^2 sec

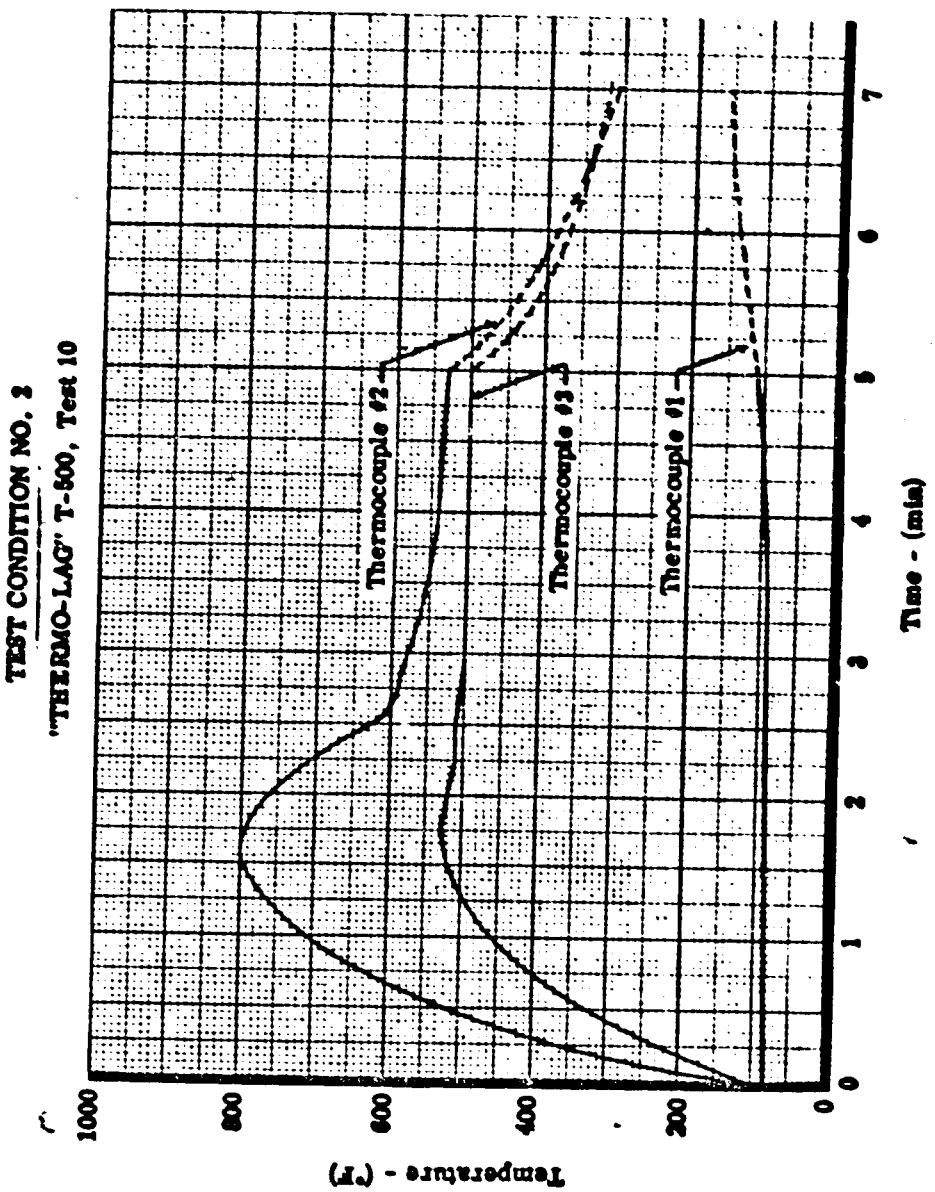

Figure 32. Thermocouple Traces, Model 9B

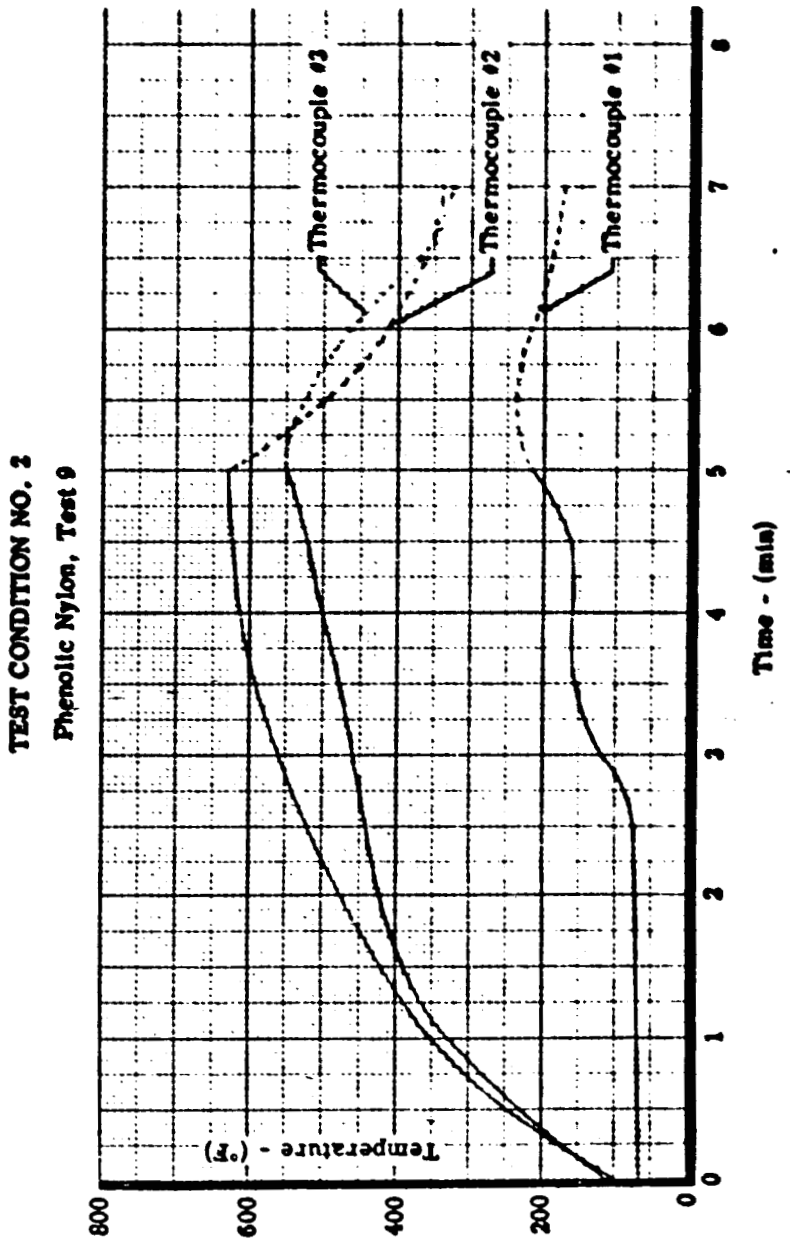

Figure 33. Thermocouple Traces, Model 13D

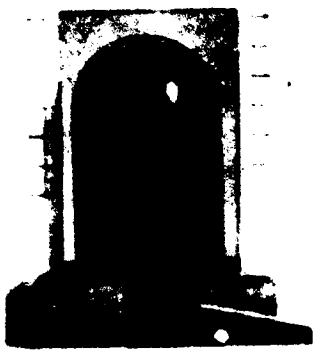

Before

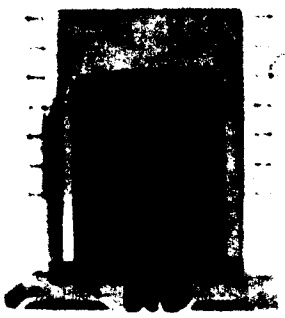

After

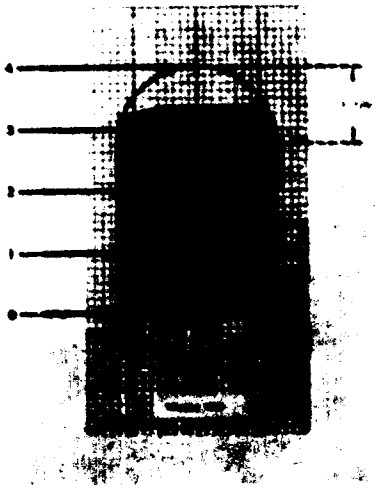

Sectioned View

Figure 34. "THERMO-LAG" T-500 Model 10D, 5-Minute Exposure to a Stagnation Enthalpy of 17,475 BTU/lb at a Heat Flux of 362.6 BTU/ft^2 sec

Before

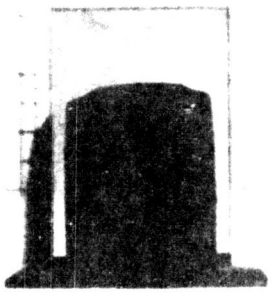

After

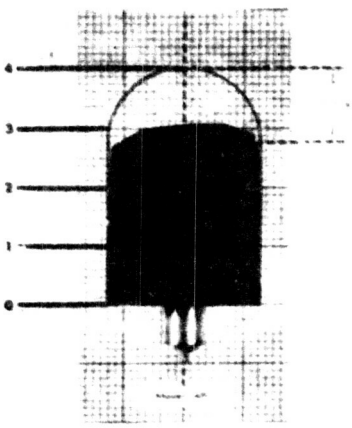

Sectioned View

Figure 35. Phenolic Nylon Model 14F, 5-Minute Exposure to a Stagnation Enthalpy of 17,565 BTU/Lb. at a Heat Flux of 354.7 BTU/Ft.^{2} Sec.

Before

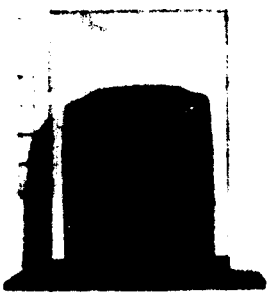

After

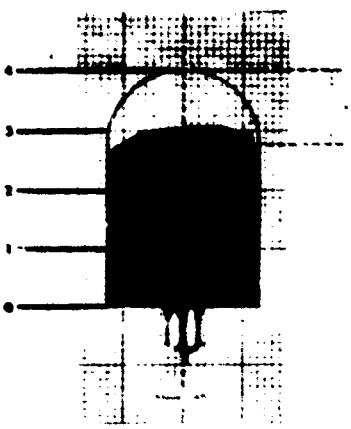

Sectioned View

Figure 35. Phenolic Nylon Model 14F, 5-Minute Exposure to a Stagnation Enthalpy of 17,565 BTU/Lb. at a Heat Flux of 354.7 BTU/Ft.^{2} Sec.

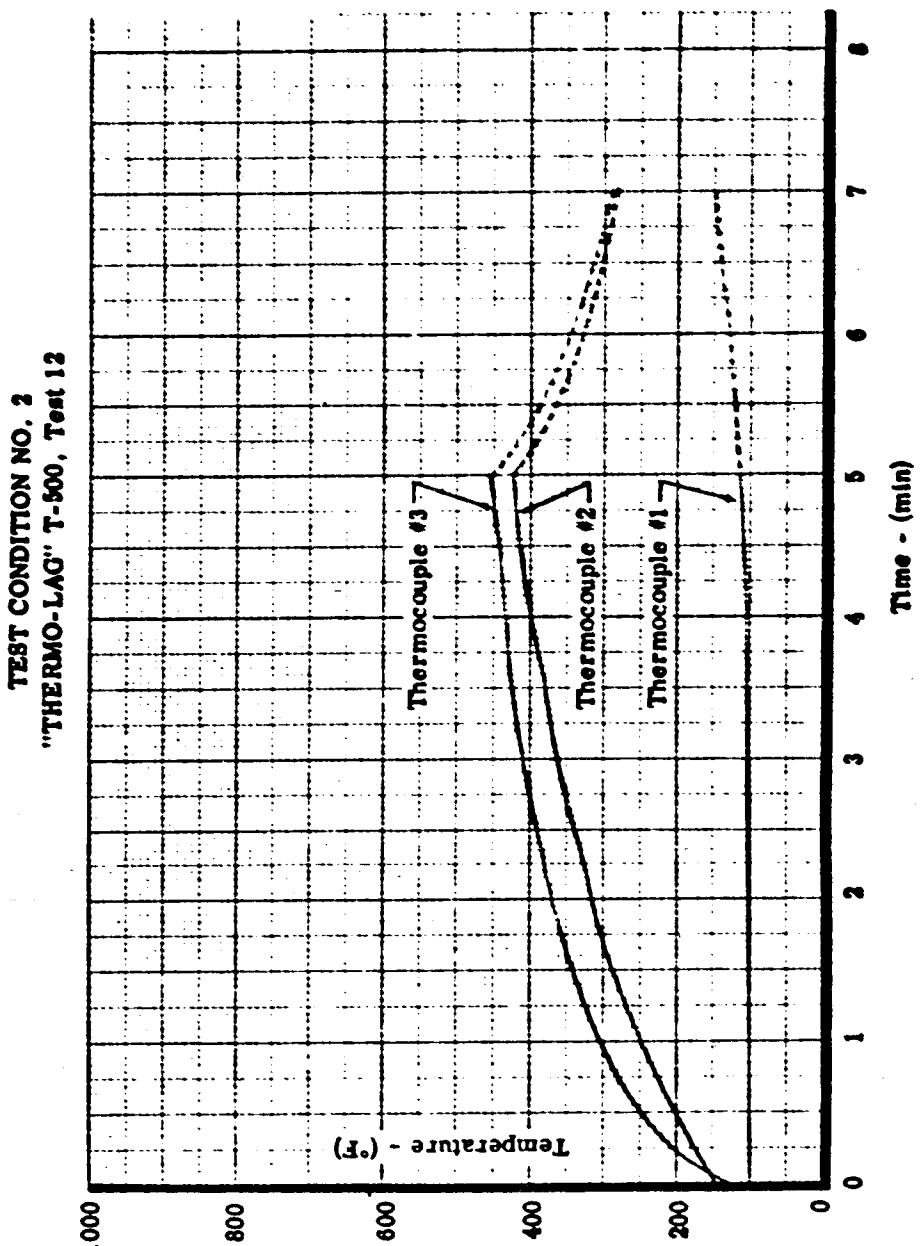

Figure 36. Thermocouple Traces, Model 10D

TEST CONDITION NO. 2

Phenolic Nylon, Test 11

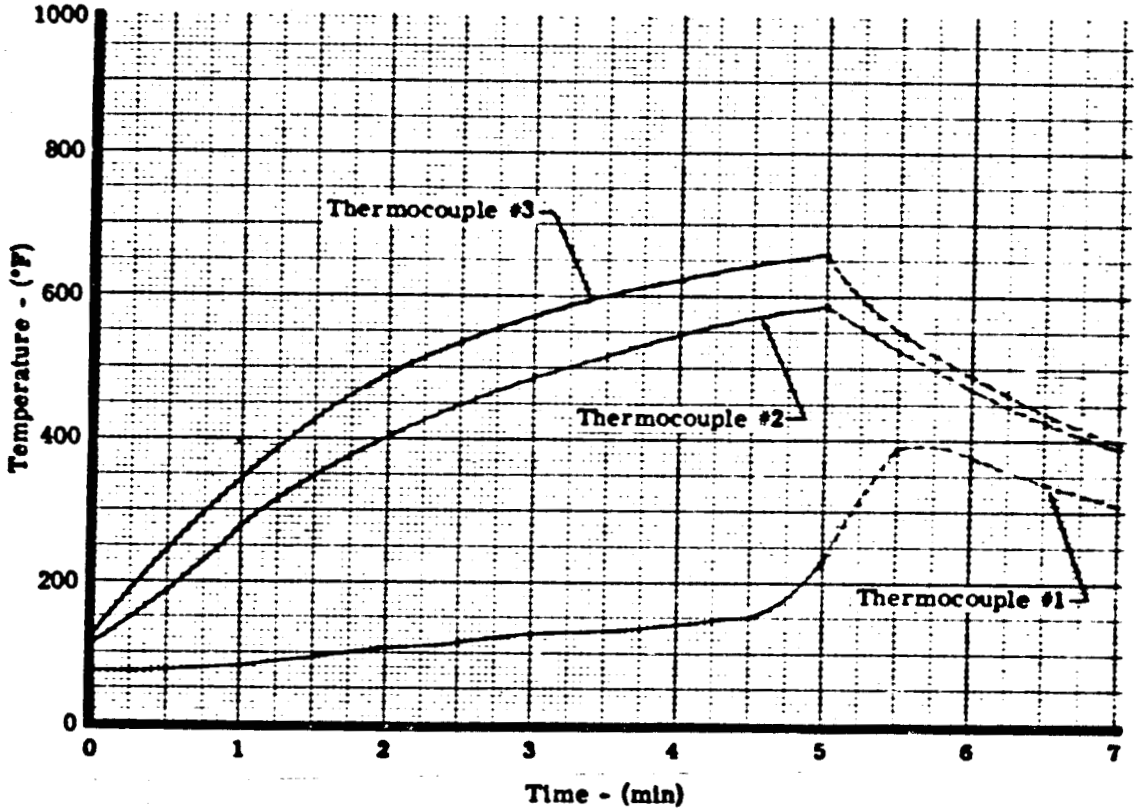

Figure 37. Thermocouple Traces, Model 14F

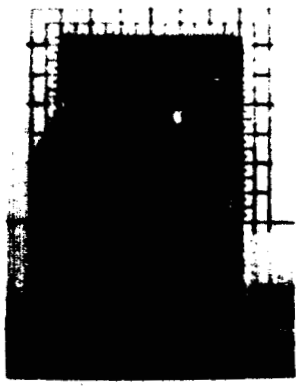

Before

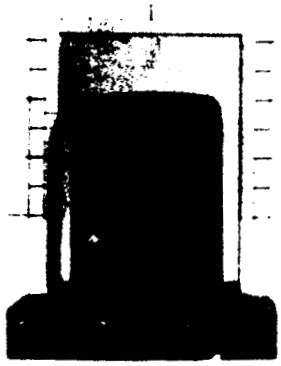

After

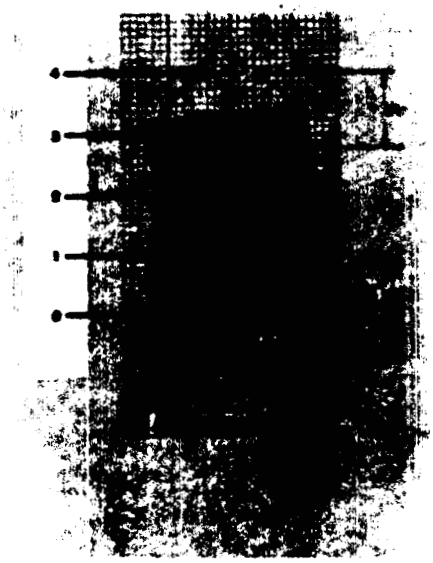

Sectioned View

Figure 38. "THERMO-LAG" T-500 Model 18A, 5-Minute Exposure to a Stagnation Enthalpy of 17,465 BTU/lb at a Heat Flux of 362.8 BTU ft^2 sec

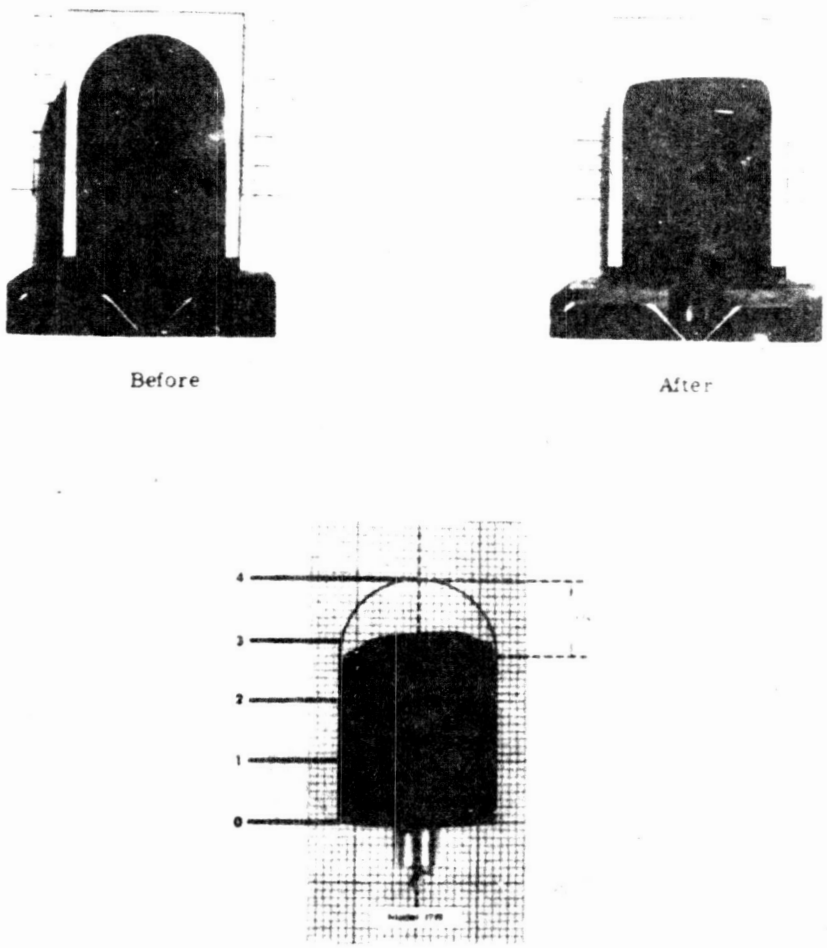

Figure 39. Phenolic Nylon Model 17B, 5-Minute Exposure to a Stagnation Enthalpy of 17,500 BTU/lb at a Heat Flux of 354.5 BTU ft^2 sec

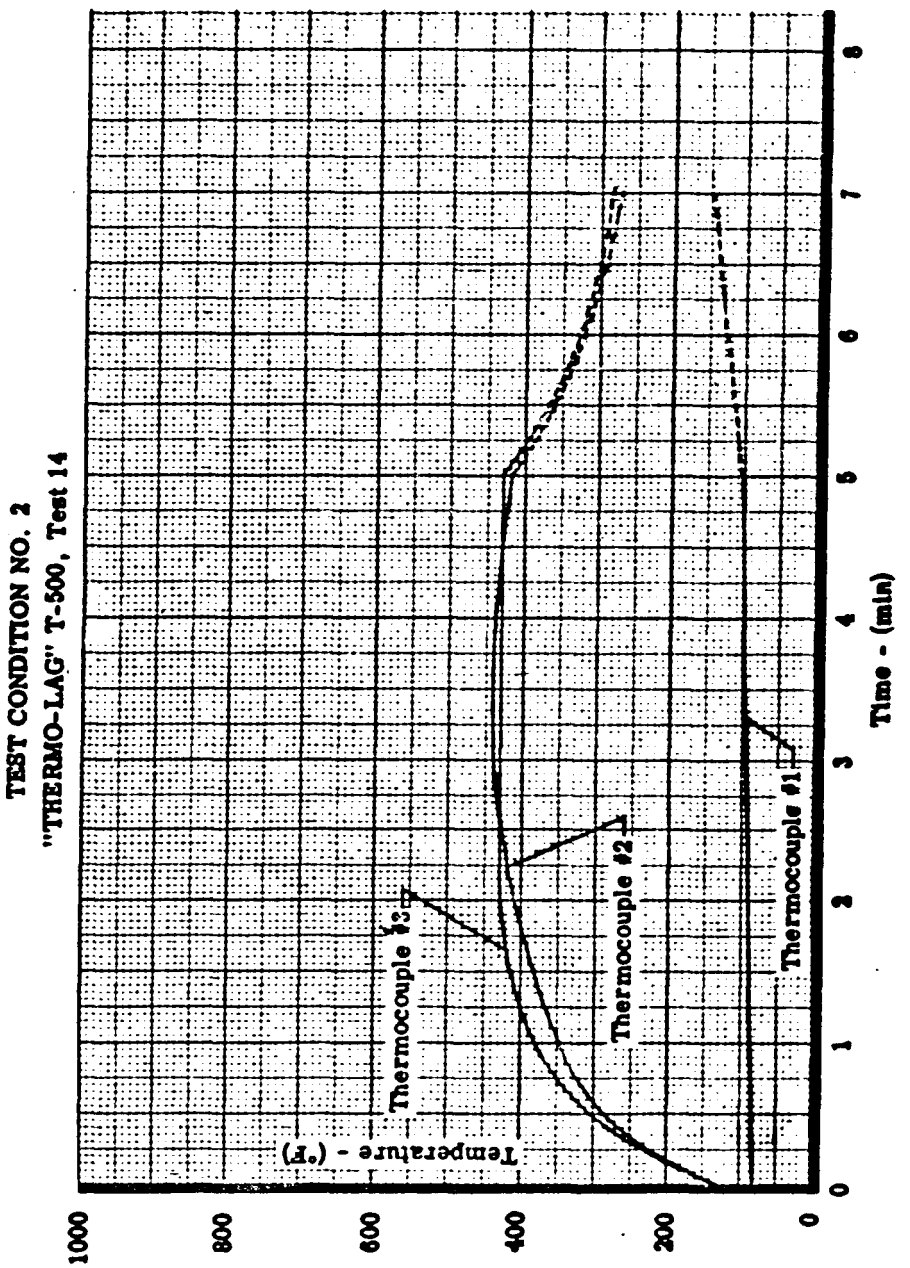

Figure 40. Thermocouple Traces, Model 18A

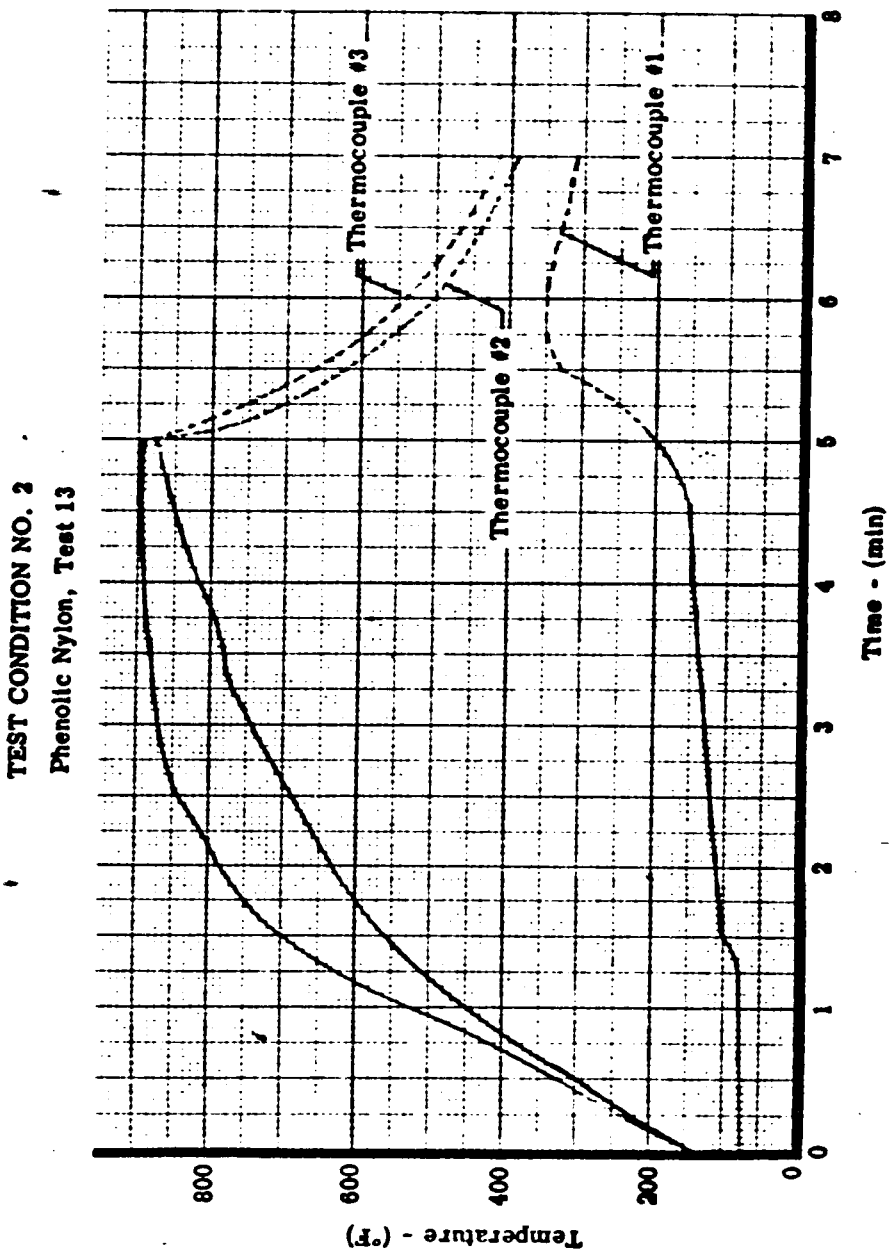

Figure 41. Thermocouple Traces, Model 17B

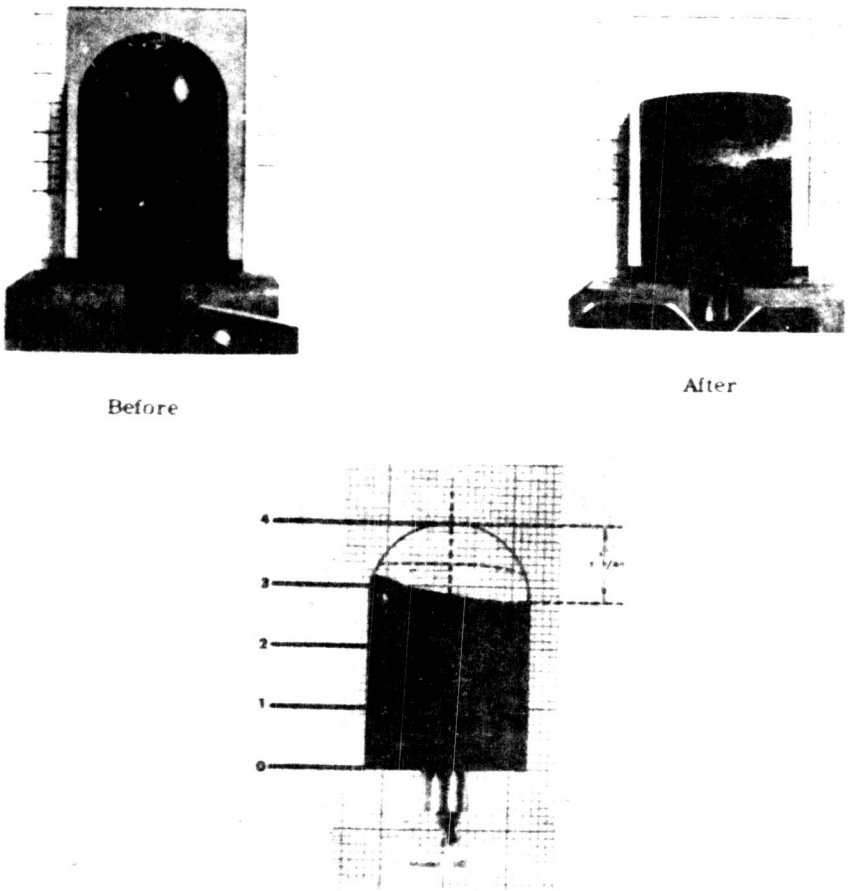

Figure 42. "THERMO-LAG" T-500 Model 11E, 11-Minute Exposure to a Stagnation Enthalpy of 17,585 BTU/lb at a Heat Flux of 362.7 BTU/ft^2 sec (Dotted Surface Indicates Model Shape After 5 Minutes of Exposure)

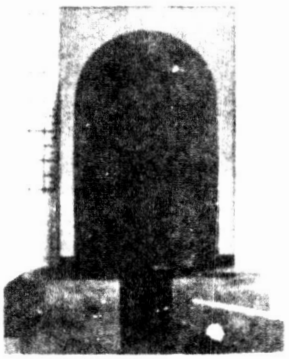

Before

After

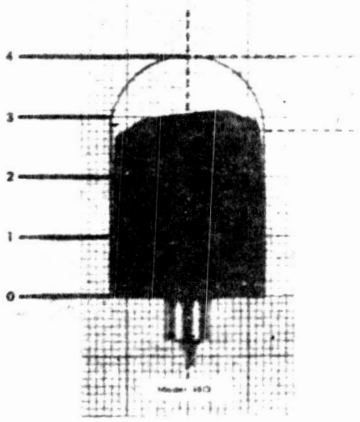

Sectioned View

Figure 43. Phenolic Nylon Model 15G, 5-Minute Exposure to a Stagnation Enthalpy of 17,389 BTU/lb at a Heat Flux of 354.3 BTU/ft^2 sec

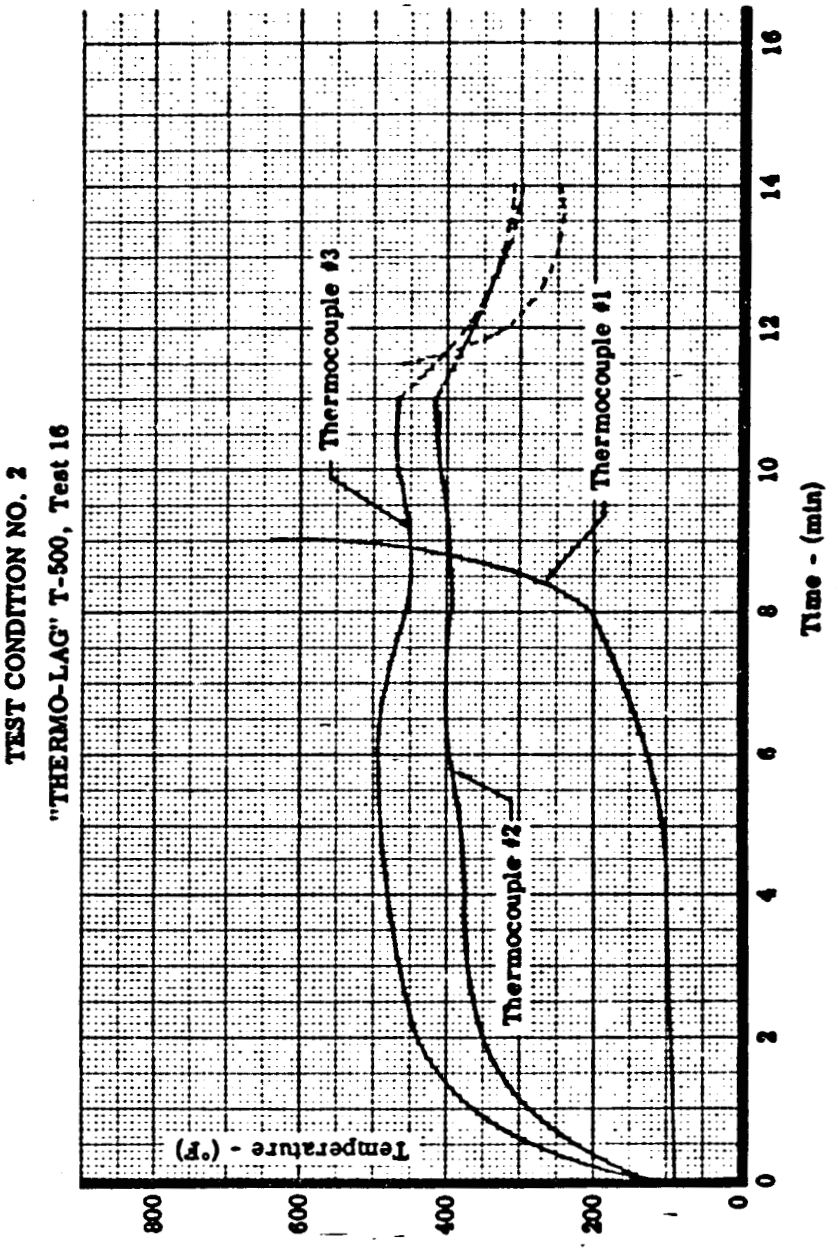

Figure 44. Thermocouple Traces, Model 11E

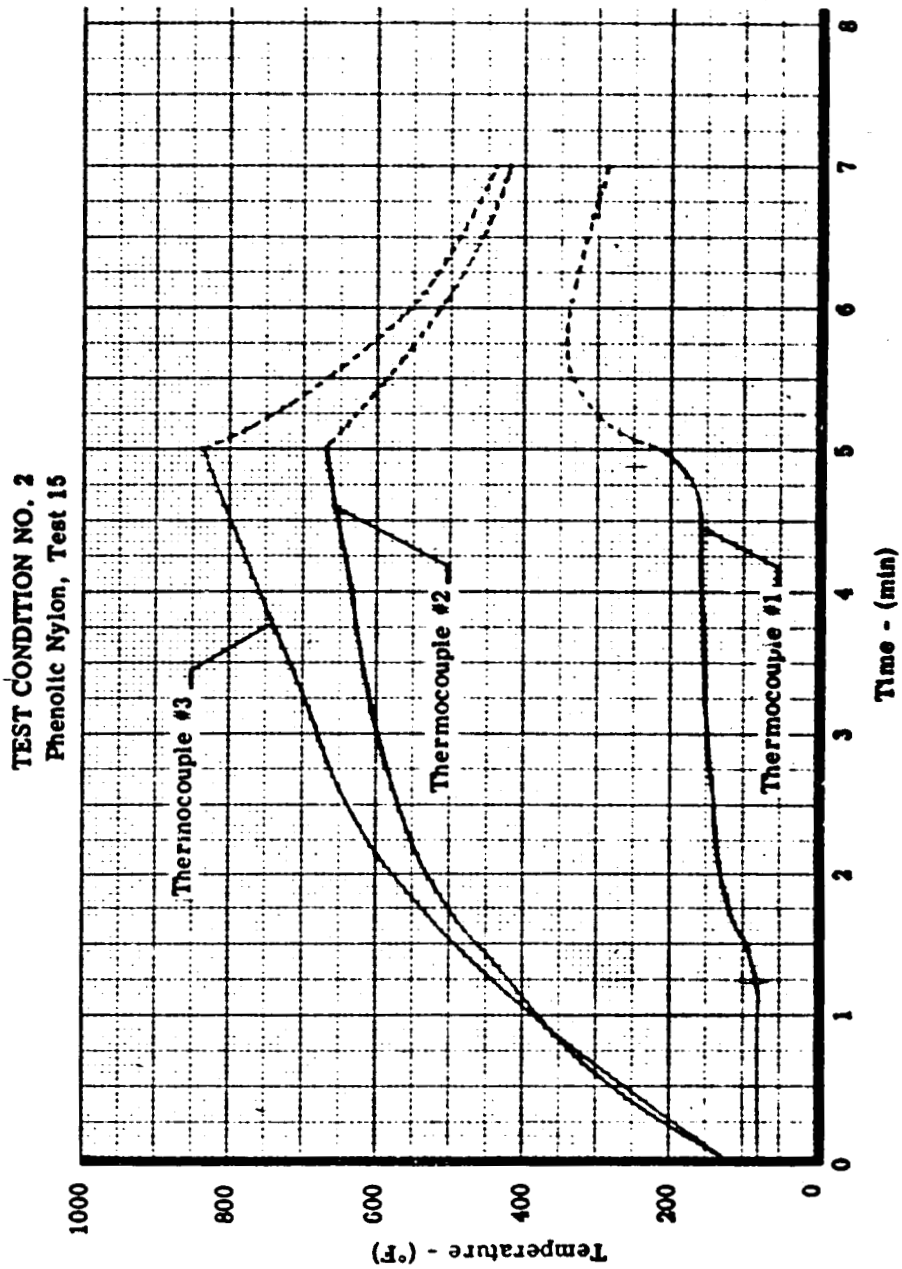

Figure 45. Thermocouple Traces, Model 15G

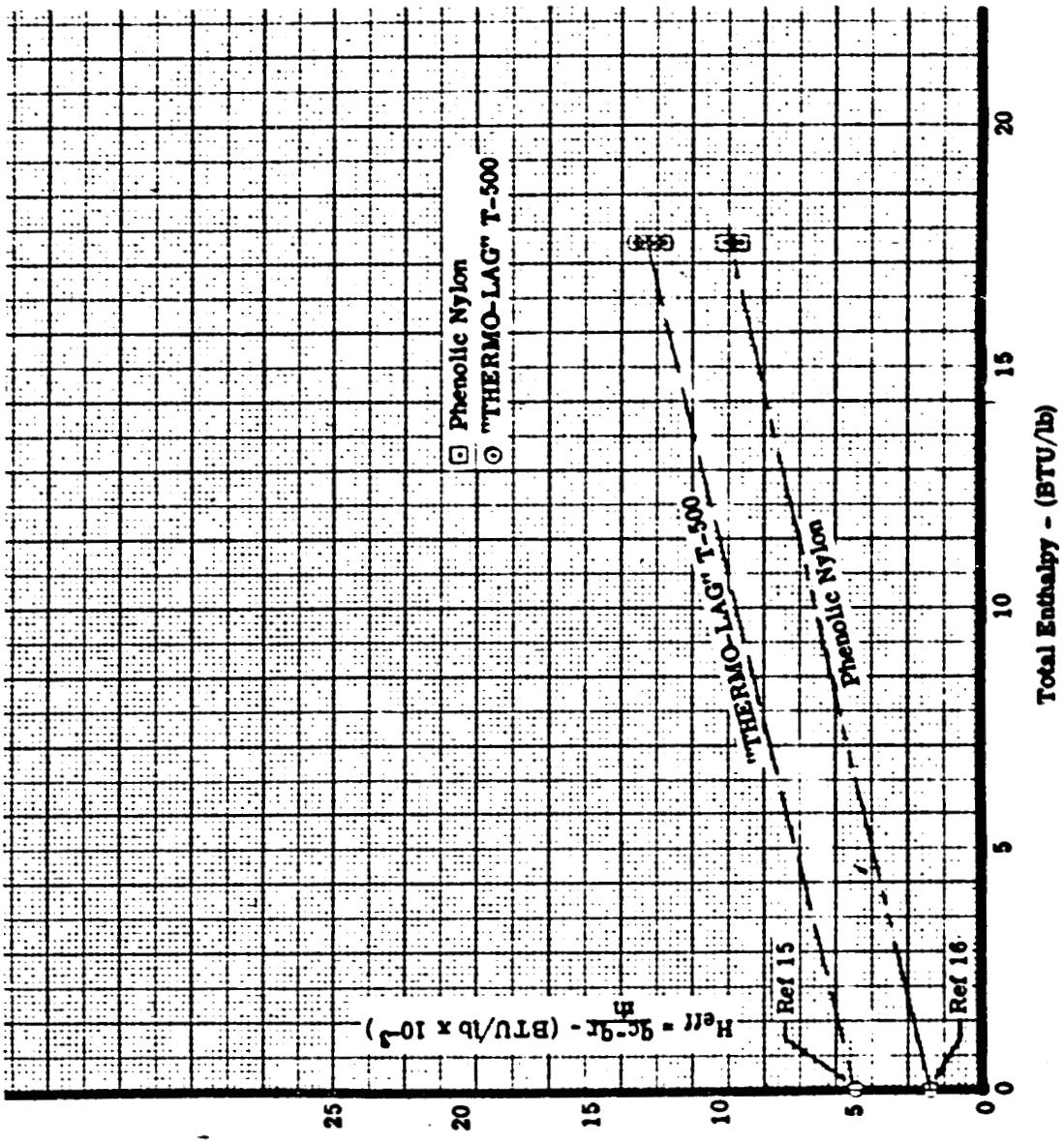

Figure 46. Heat Blockage as a Function of Total Enthalpy

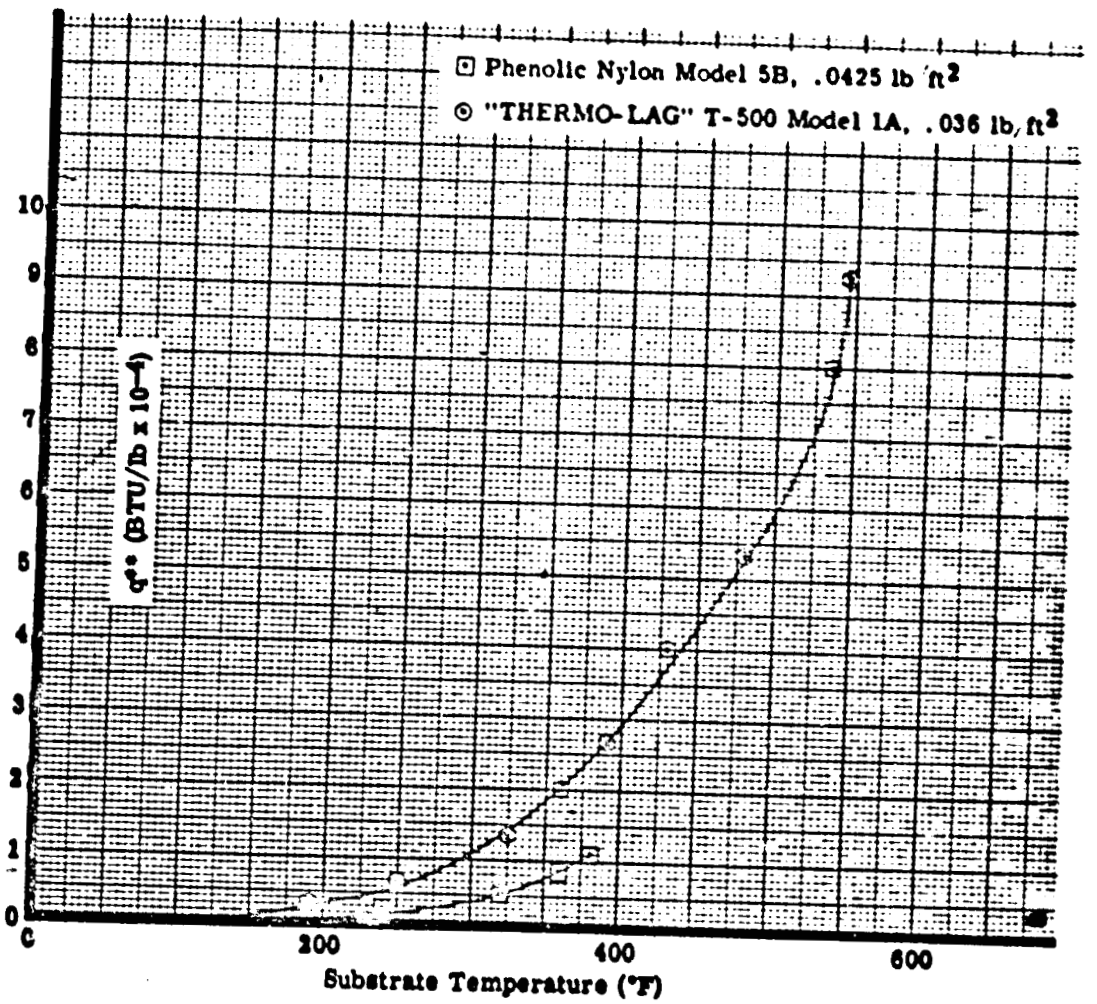

Figure 47. Material Evaluation Curve

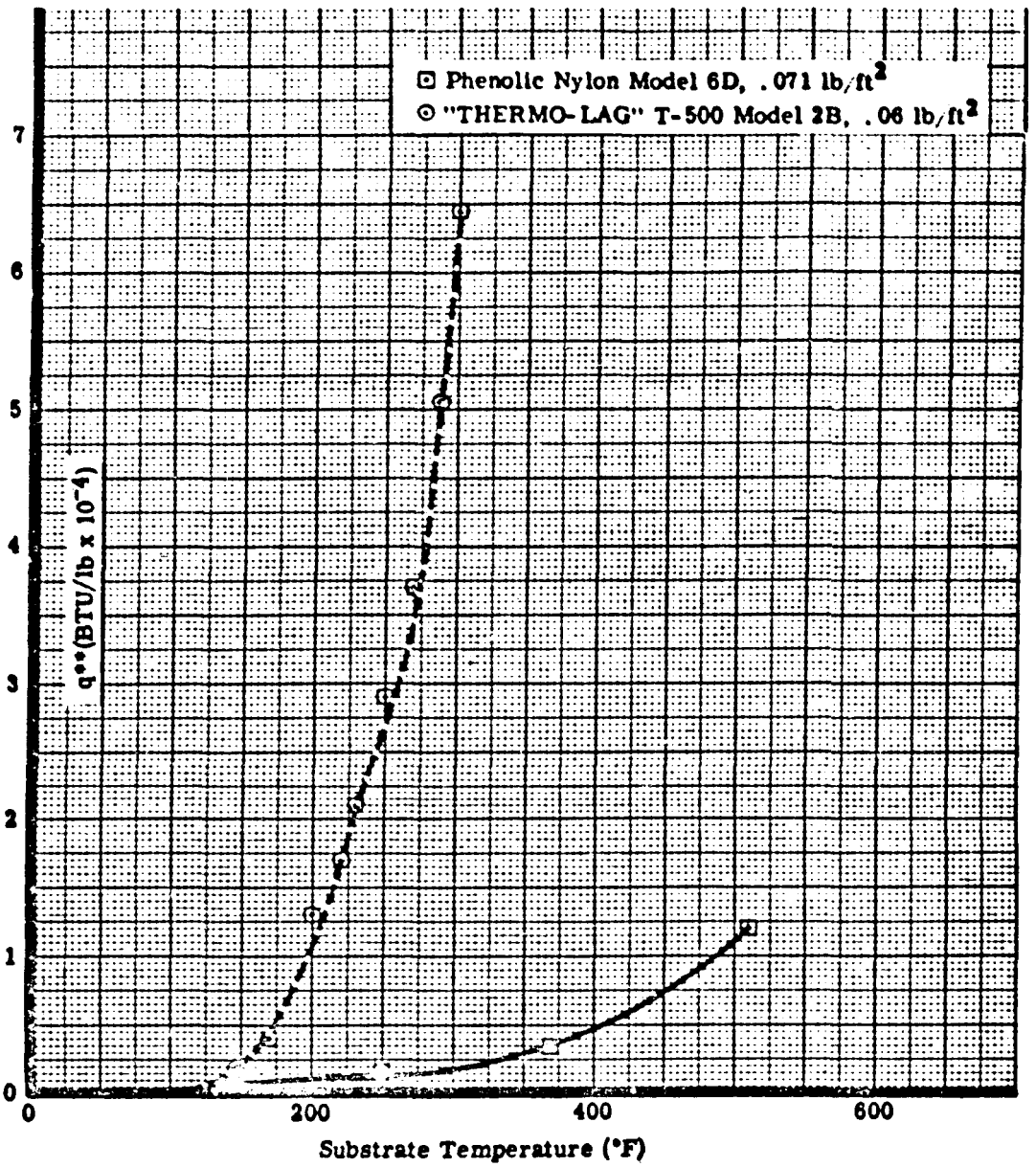

Figure 48. Material Evaluation Curve

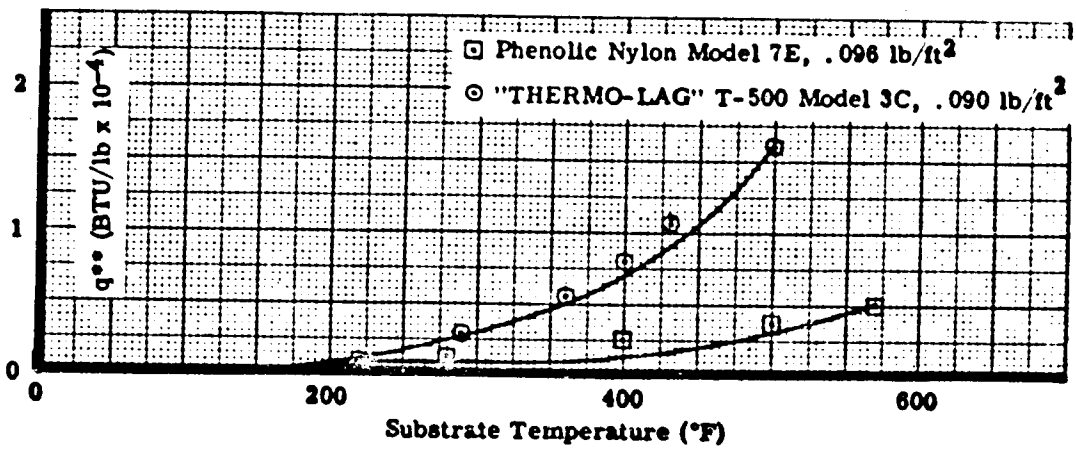

Figure 49. Material Evaluation Curve

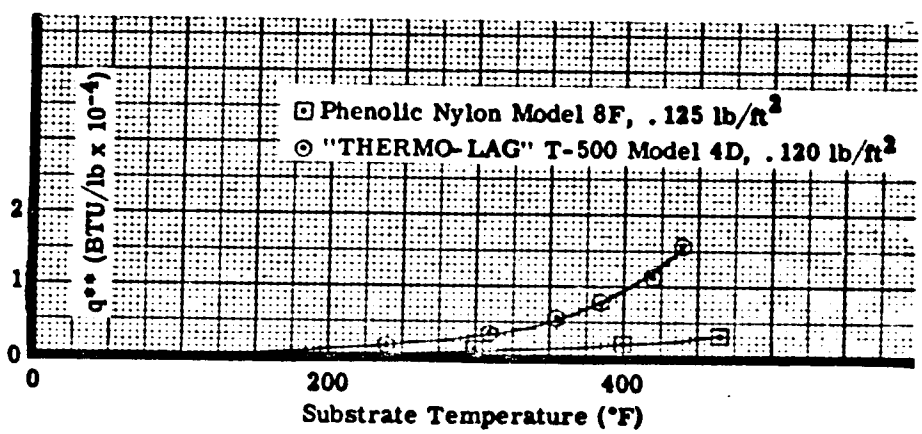

Figure 50. Material Evaluation Curve

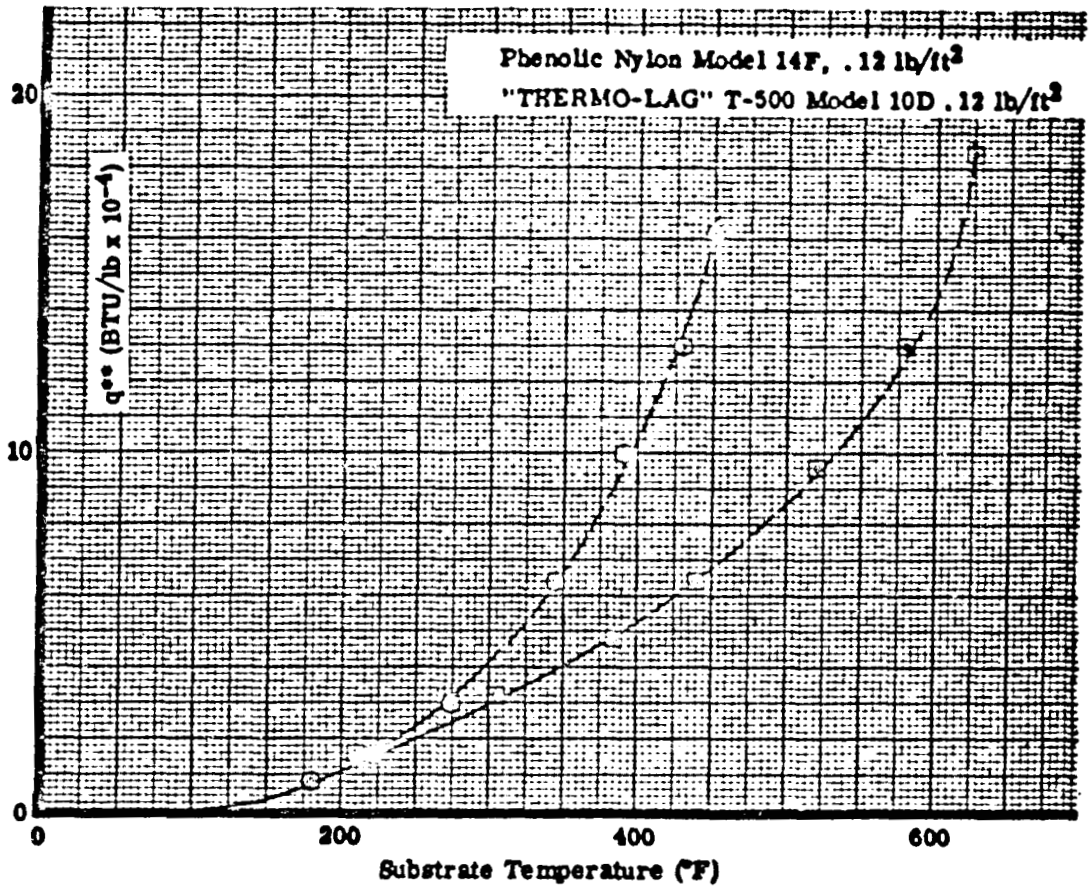

Figure 51. Material Evaluation Curve

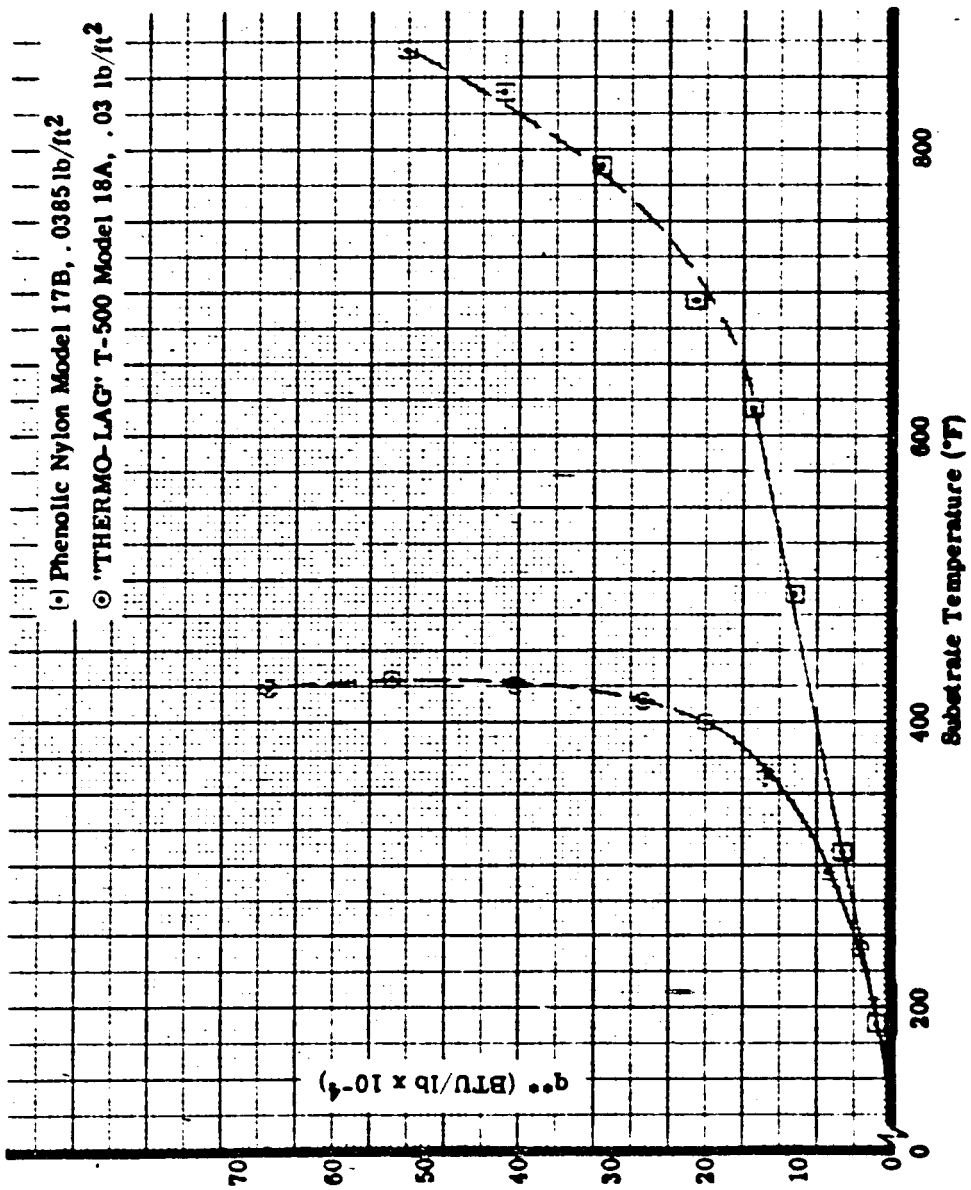

Figure 52.. Material Evaluation Curve

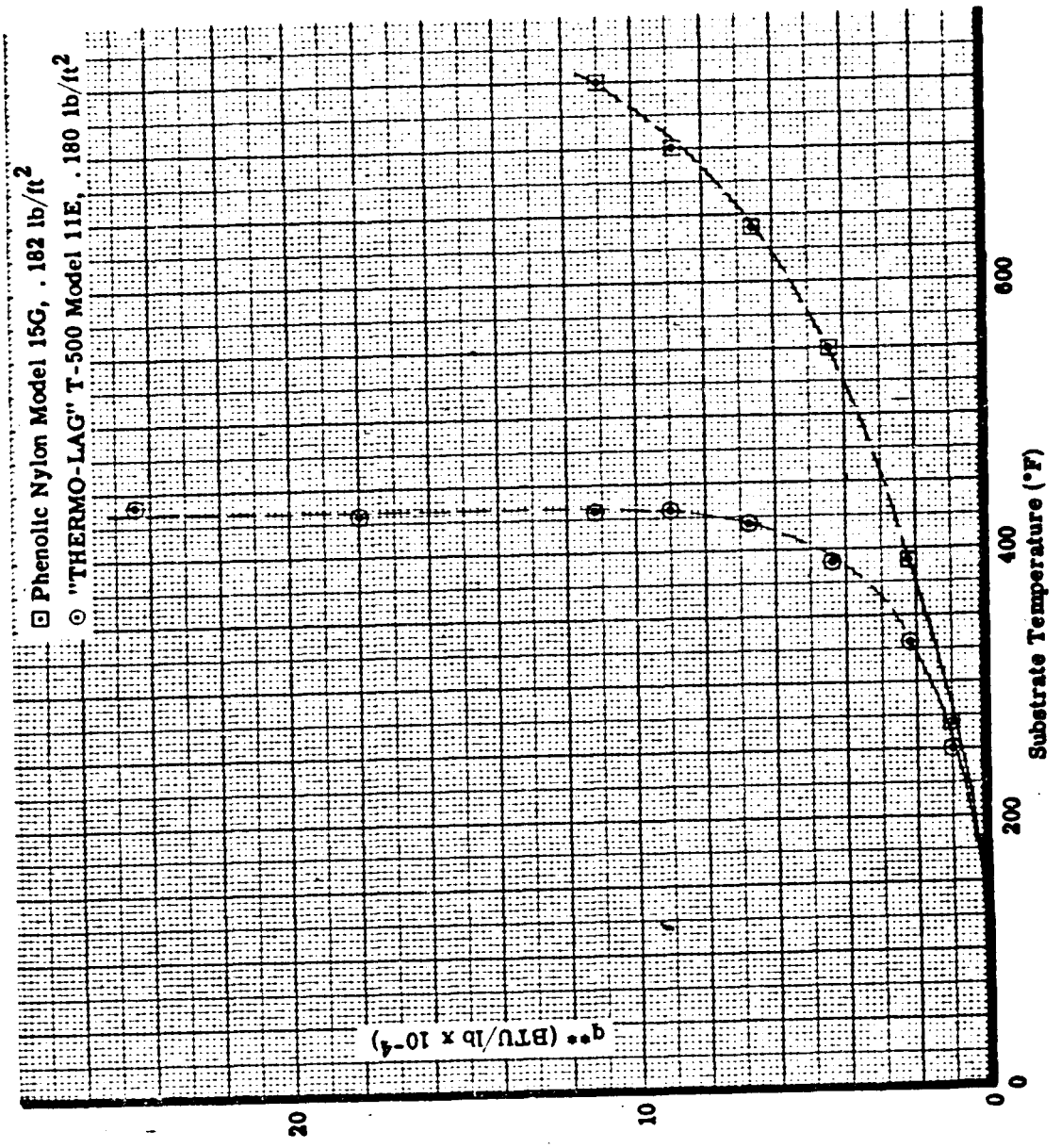

Figure 53. Material Evaluation Curve

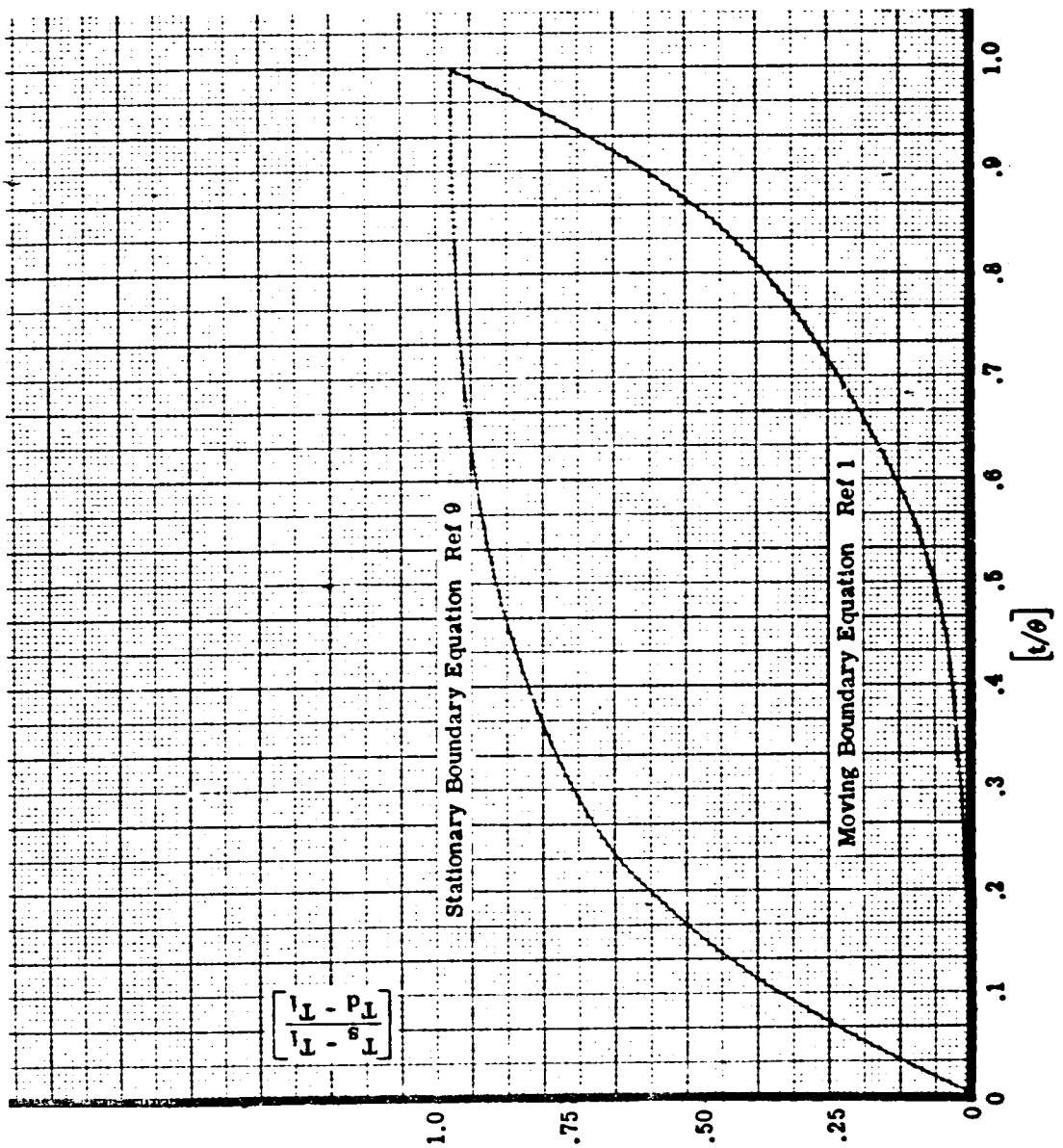

Figure 54. Substrate Temperature Histories for Stationary and Moving Boundary Equations

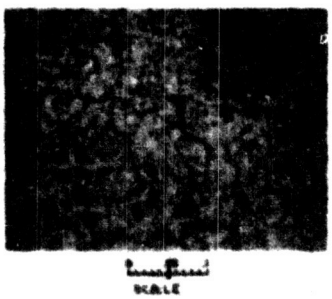

Figure 55. Photomicrograph (6.5X) Taken .18 Inch from Surface of "THERMO-LAG" T-500 Model After One Hour Exposure to a Stagnation Enthalpy of 3,500 BTU/lb at a Heat Flux of 33 BTU/ft^2 sec

REFERENCES

1. "The Ablation of Reinforced Plastics in Supersonic Flow", George W. Sutton, General Electric paper 57SD644, July 1957.

2. "The Use of Ablators for Achieving Protection Against High Thermal Flux", Kenneth L. Wadlin, Joseph N. Kotanchik, Society of Automotive Engineers paper 417C, October 1961.

3. "Properties of "THERMO-LAG" T-500 EX 167 Subliming Compound", Emerson Electric Manufacturing Company, Report 1136.

4. "Telecon to Emerson Electric from NASA", Langley Field, Virginia. Concerning the thermal properties of low-density phenolic nylon.

5. "Convective Heat Transfer with Mass Addition and Chemical Reactions", Lester Lees, Combustion and Propulsion, Third AGARD Colloquium.

6. "Thermodynamic Coupling in Boundary Layers", Judson R. Baron, American Rocket Society Journal, July 1962, pp 1053-59.

7. "On the Coupling Between Heat and Mass Transfer", O.E. Tewfik, C. J. Shirliffe, Journal of the Aerospace Sciences, August 1962, pp 1009-10.

8. "Thermal Effects on a Transpiration Cooled Hemisphere", Albert F. Gallnick, Jr., Journal of the Aerospace Sciences, May 1962, pp 583-90.

9. "S.A.E. Applied Aerospace Thermodynamics Manual", Revision of January 1962.

10. "Recent Advances in Ablation", Marc C. Adams, American Rocket Society Journal, September 1959, pp 625-32.

11. "Effects of Surface Recombination on Heat Transfer to Bodies in a High Enthalpy Stream of Partially Dissociated Nitrogen", Ernest L. Winkler, Roy N. Griffen, Jr., NASA TN D-1146, December 1961.

12. "On Catalytic Recombination Rates in Hypersonic Stagnation Heat Transfer", Robert J. Goulard, Jet Propulsion, November 1958, pp 737-45.

13. "The Downstream Influence of Mass Transfer at the Nose of a Slender Cone", Robert J. Cresci, Paul A. Libby, Journal of the Aerospace Sciences, July 1962, pp 815-26.

14. "Effects of Carbon Contamination of Air on Ablation Arc Wind Tunnel Test Results", S. Georgiev, P. H. Rose, AVCO Research Report 113, December 1959.

15. "Properties of "THERMO-LAG" T-500 EX 167 Subliming Compound", an Emerson Electric Report to be published, Revision of Reference 3.

16. "Materials for Re-Entry Heat Protection of Satellites", presented at ARS Semi-annual Meeting, San Diego, June 1959, by L Steg.